Since January 2020 Elsevier has created a COVID-19 resource centre with free information in English and Mandarin on the novel coronavirus COVID-19. The COVID-19 resource centre is hosted on Elsevier Connect, the company's public news and information website.

Article

Cell

Structure, Function, and Antigenicity of the SARS-CoV-2 Spike Glycoprotein

Graphical Abstract

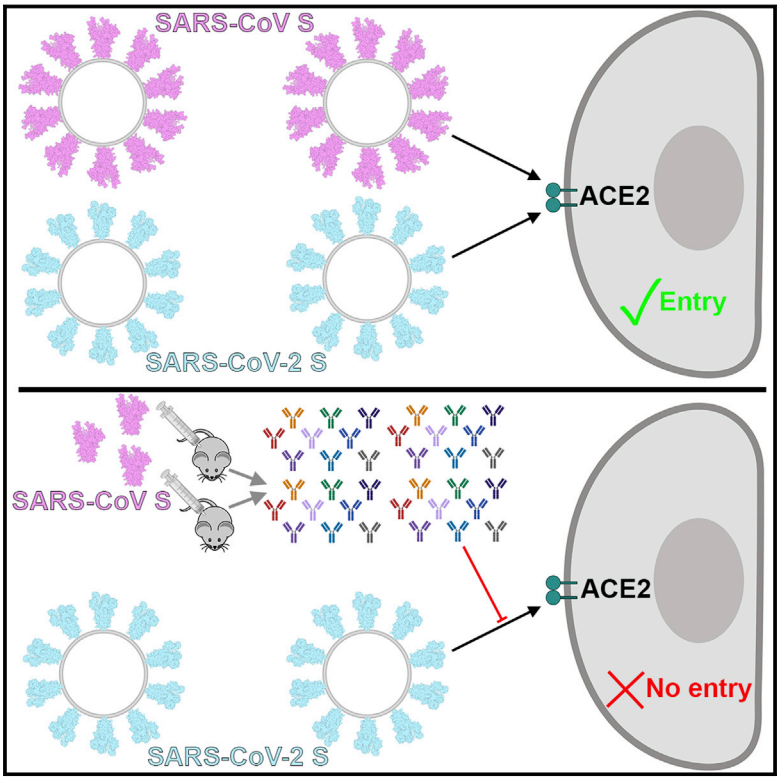

Authors

Alexandra C. Walls, Young-Jun Park, M. Alejandra Tortorici, Abigail Wall, Andrew T. McGuire, David Veesler

Correspondence

dveesler@uw.edu

In Brief

SARS-CoV-2, a newly emerged pathogen spreading worldwide, binds with high affinity to human ACE2 and uses it as an entry receptor to invade target cells. Cryo-EM structures of the SARS-CoV-2 spike glycoprotein in two distinct conformations, along with inhibition of spike-mediated entry by SARS-CoV polyclonal antibodies, provide a blueprint for the design of vaccines and therapeutics.

Highlights

- SARS-CoV-2 uses ACE2 to enter target cells
- SARS-CoV-2 and SARS-CoV bind with similar affinities to ACE2
- Structures of SARS-CoV-2 spike glycoprotein in two conformations
- SARS-CoV polyclonal antibodies inhibit SARS-CoV-2 spike-mediated entry into cells

Walls et al., 2020, Cell *180*, 281–292
April 16, 2020
https://doi.org/10.1016/j.cell.2020.02.058

CellPress

Article

Cell

Structure, Function, and Antigenicity of the SARS-CoV-2 Spike Glycoprotein

Alexandra C. Walls,[1,5] Young-Jun Park,[1,5] M. Alejandra Tortorici,[1,2] Abigail Wall,[3] Andrew T. McGuire,[3,4] and David Veesler[1,6,*]

[1]Department of Biochemistry, University of Washington, Seattle, WA 98195, USA
[2]Institute Pasteur & CNRS UMR 3569, Unité de Virologie Structurale, Paris 75015, France
[3]Vaccines and Infectious Diseases Division, Fred Hutchinson Cancer Research Center, Seattle, WA 98195, USA
[4]Department of Global Health, University of Washington, Seattle, WA 98195, USA
[5]These authors contributed equally
[6]Lead Contact
*Correspondence: dveesler@uw.edu
https://doi.org/10.1016/j.cell.2020.02.058

SUMMARY

The emergence of SARS-CoV-2 has resulted in >90,000 infections and >3,000 deaths. Coronavirus spike (S) glycoproteins promote entry into cells and are the main target of antibodies. We show that SARS-CoV-2 S uses ACE2 to enter cells and that the receptor-binding domains of SARS-CoV-2 S and SARS-CoV S bind with similar affinities to human ACE2, correlating with the efficient spread of SARS-CoV-2 among humans. We found that the SARS-CoV-2 S glycoprotein harbors a furin cleavage site at the boundary between the S_1/S_2 subunits, which is processed during biogenesis and sets this virus apart from SARS-CoV and SARS-related CoVs. We determined cryo-EM structures of the SARS-CoV-2 S ectodomain trimer, providing a blueprint for the design of vaccines and inhibitors of viral entry. Finally, we demonstrate that SARS-CoV S murine polyclonal antibodies potently inhibited SARS-CoV-2 S mediated entry into cells, indicating that cross-neutralizing antibodies targeting conserved S epitopes can be elicited upon vaccination.

INTRODUCTION

Three coronaviruses have crossed the species barrier to cause deadly pneumonia in humans since the beginning of the 21st century: severe acute respiratory syndrome coronavirus (SARS-CoV) (Drosten et al., 2003; Ksiazek et al., 2003), Middle-East respiratory syndrome coronavirus (Zaki et al., 2012) (MERS-CoV), and SARS-CoV-2 (Huang et al., 2020; Zhu et al., 2020). SARS-CoV emerged in the Guangdong province of China in 2002 and spread to five continents through air travel routes, infecting 8,098 people and causing 774 deaths. In 2012, MERS-CoV emerged in the Arabian Peninsula, where it remains a major public health concern, and was exported to 27 countries, infecting a total of ~2,494 individuals and claiming 858 lives. A previously unknown coronavirus, named SARS-CoV-2, was discovered in December 2019 in Wuhan, Hubei province of China and was sequenced and isolated by January 2020 (Zhou et al., 2020; Zhu et al., 2020). SARS-CoV-2 is associated with an ongoing outbreak of atypical pneumonia (Covid-2019) that has affected over 90,000 people and killed more than 3,000 of those affected in >60 countries as of March 3, 2020. On January 30, 2020, the World Health Organization declared the SARS-CoV-2 epidemic a public health emergency of international concern.

MERS-CoV was suggested to originate from bats, but the reservoir host fueling spillover to humans is unequivocally dromedary camels (Haagmans et al., 2014; Memish et al., 2013). Both SARS-CoV and SARS-CoV-2 are closely related and originated in bats, who most likely serve as reservoir host for these two viruses (Ge et al., 2013; Hu et al., 2017; Li et al., 2005b; Yang et al., 2015a; Zhou et al., 2020). Whereas palm civets and racoon dogs have been recognized as intermediate hosts for zoonotic transmission of SARS-CoV between bats and humans (Guan et al., 2003; Kan et al., 2005; Wang et al., 2005), the SARS-CoV-2 intermediate host remains unknown. The recurrent spillovers of coronaviruses in humans along with detection of numerous coronaviruses in bats, including many SARS-related coronaviruses (SARSr-CoVs), suggest that future zoonotic transmission events may continue (Anthony et al., 2017; Ge et al., 2013; Hu et al., 2017; Li et al., 2005b; Menachery et al., 2015; Menachery et al., 2016; Yang et al., 2015a; Zhou et al., 2020). In addition to the highly pathogenic zoonotic pathogens SARS-CoV, MERS-CoV, and SARS-CoV-2, all belonging to the β-coronavirus genus, four low-pathogenicity coronaviruses are endemic in humans: HCoV-OC43, HCoV-HKU1, HCoV-NL63, and HCoV-229E. To date, no therapeutics or vaccines are approved against any human-infecting coronaviruses.

Coronavirus entry into host cells is mediated by the transmembrane spike (S) glycoprotein that forms homotrimers protruding from the viral surface (Tortorici and Veesler, 2019). S comprises two functional subunits responsible for binding to the host cell receptor (S_1 subunit) and fusion of the viral and cellular membranes (S_2 subunit). For many CoVs, S is cleaved at the boundary between the S_1 and S_2 subunits, which remain non-covalently bound in the prefusion conformation (Belouzard et al., 2009; Bosch et al., 2003; Burkard et al., 2014; Kirchdoerfer et al., 2016; Millet and Whittaker, 2014,

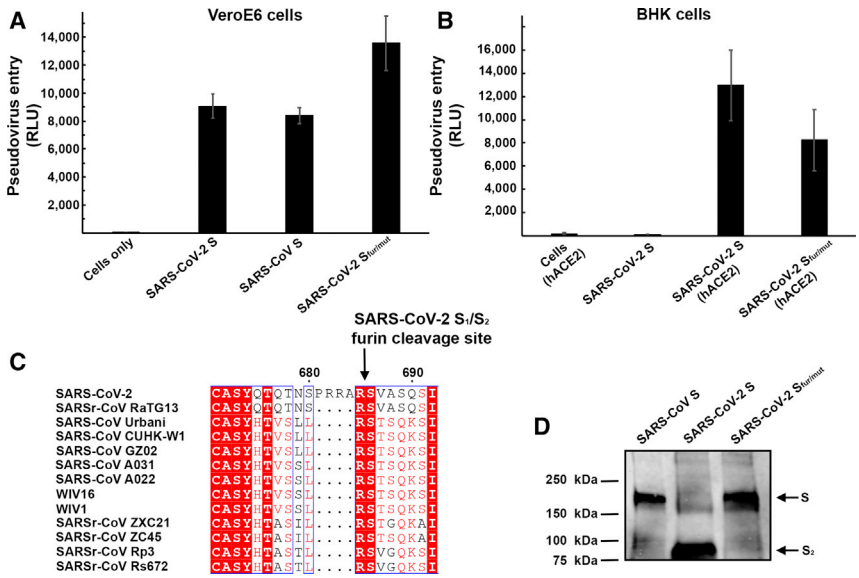

Figure 1. ACE2 Is a Functional Receptor for SARS-CoV-2 S

(A) Entry of MLV pseudotyped with SARS-CoV-2 S, SARS-CoV S and SARS-CoV-2 $S_{fur/mut}$ in VeroE6 cells. Data are represented as mean ± standard deviation of technical triplicates.

(B) Entry of MLV pseudotyped with SARS-CoV-2 S or SARS-CoV-2 $S_{fur/mut}$ in BHK cells transiently transfected with hACE2. The experiments were carried out with two independent pseudovirus preparations and a representative experiment is shown. Data are represented as mean ± standard deviation of technical triplicates.

(C) Sequence alignment of SARS-CoV-2 S with multiple related SARS-CoV and SARSr-CoV S glycoproteins reveals the introduction of an S_1/S_2 furin cleavage site in this novel coronavirus. Identical and similar positions are respectively shown with white or red font. The four amino acid residue insertion at SARS-CoV-2 S positions 681-684 is indicated with periods. The entire sequence alignment is presented in Data S1.

(D) Western blot analysis of SARS-CoV S-MLV, SARS-CoV-2 S-MLV, and SARS-CoV-2 $S_{fur/mut}$-MLV pseudovirions. See also Data S1.

2015; Park et al., 2016; Walls et al., 2016a). The distal S_1 subunit comprises the receptor-binding domain(s) and contributes to stabilization of the prefusion state of the membrane-anchored S_2 subunit that contains the fusion machinery (Gui et al., 2017; Kirchdoerfer et al., 2016; Pallesen et al., 2017; Song et al., 2018; Walls et al., 2016a; Walls et al., 2017b; Yuan et al., 2017). For all CoVs, S is further cleaved by host proteases at the so-called S_2' site located immediately upstream of the fusion peptide (Madu et al., 2009; Millet and Whittaker, 2015). This cleavage has been proposed to activate the protein for membrane fusion via extensive irreversible conformational changes (Belouzard et al., 2009; Heald-Sargent and Gallagher, 2012; Millet and Whittaker, 2014, 2015; Park et al., 2016; Walls et al., 2017b). As a result, coronavirus entry into susceptible cells is a complex process that requires the concerted action of receptor-binding and proteolytic processing of the S protein to promote virus-cell fusion.

Different coronaviruses use distinct domains within the S_1 subunit to recognize a variety of attachment and entry receptors, depending on the viral species. Endemic human coronaviruses OC43 and HKU1 attach via their S domain A (S^A) to 5-N-acetyl-9-*O*-acetyl-sialosides found on glycoproteins and glycolipids at the host cell surface to enable entry into susceptible cells (Hulswit et al., 2019; Tortorici et al., 2019; Vlasak et al., 1988). MERS-CoV S, however, uses domain A to recognize non-acetylated sialoside attachment receptors (Li et al., 2017; Park et al., 2019), which likely promote subsequent binding of domain B (S^B) to the entry receptor, dipeptidyl-peptidase 4 (Lu et al., 2013; Raj et al., 2013). SARS-CoV and several SARS-related coronaviruses (SARSr-CoV) interact directly with angiotensin-converting enzyme 2 (ACE2) via S^B to enter target cells (Ge et al., 2013; Kirchdoerfer et al., 2018; Li et al., 2005a; Li et al., 2003; Song et al., 2018; Yang et al., 2015a).

As the coronavirus S glycoprotein is surface-exposed and mediates entry into host cells, it is the main target of neutralizing antibodies (Abs) upon infection and the focus of therapeutic and vaccine design. S trimers are extensively decorated with N-linked glycans that are important for proper folding (Rossen et al., 1998) and for modulating accessibility to host proteases and neutralizing Abs (Walls et al., 2016b; Walls et al., 2019; Xiong et al., 2018; Yang et al., 2015b). We previously characterized potent human-neutralizing Abs from rare memory B cells of individuals infected with SARS-CoV (Traggiai et al., 2004) or MERS-CoV (Corti et al., 2015) in complex with SARS-CoV S and MERS-CoV S to provide molecular-level information of the mechanism of competitive inhibition of S^B attachment to the host receptor (Walls et al., 2019). The S230 anti-SARS-CoV Ab also acted by functionally mimicking receptor attachment and promoting S fusogenic conformational rearrangements through a ratcheting mechanism that elucidated the unique nature of the coronavirus membrane fusion activation (Walls et al., 2019).

We report here that ACE2 could mediate SARS-CoV-2 S-mediated entry into cells, establishing it as a functional receptor for this newly emerged coronavirus. The SARS-CoV-2 S^B engages human ACE2 (hACE2) with comparable affinity to SARS-CoV S^B from viral isolates associated with the 2002–2003 epidemic (i.e., binding with high affinity to hACE2). Tight binding to hACE2 could partially explain the efficient transmission of SARS-CoV-2 in humans, as was the case for SARS-CoV. We identified the presence of an unexpected furin cleavage site at the S_1/S_2 boundary of SARS-CoV-2 S, which is cleaved during biosynthesis—a novel feature setting this virus apart from SARS-CoV and SARSr-CoVs. Abrogation of this cleavage motif moderately affected SARS-CoV-2 S-mediated entry into VeroE6 or BHK cells but may contribute to expand the tropism of this virus, as reported for several highly pathogenic avian influenza viruses and pathogenic Newcastle disease virus (Klenk and Garten, 1994; Steinhauer, 1999). We determined cryoelectron microscopy (cryo-EM) structures of

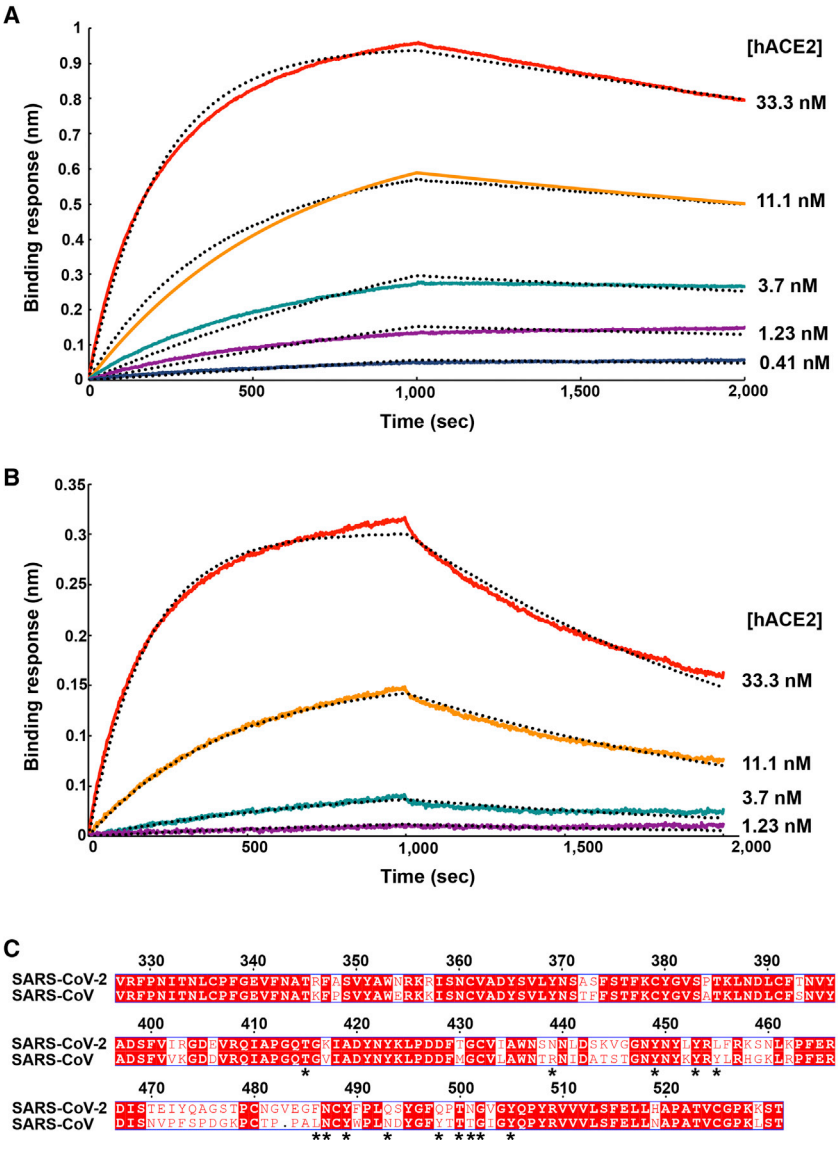

Figure 2. SARS-CoV-2 S Recognizes hACE2 with Comparable Affinity to SARS-CoV S

(A and B) Biolayer interferometry binding analysis of the hACE2 ectodomain to immobilized SARS-CoV-2 S^B (A) or SARS-CoV S^B (B). The experiments were repeated with different protein preparations and one representative set of curves is shown. Dotted lines correspond to a global fit of the data using a 1:1 binding model.

(C) Sequence alignment of SARS-CoV-2 S^B and SARS-CoV S^B Urbani (late phase of the 2002–2003 SARS-CoV epidemic). Identical and similar positions are respectively shown with white or red font. The single amino acid insertion at position 483 of the SARS-CoV-2 S^B is indicated with a period at the corresponding SARS-CoV S^B position. The 14 residues that are key for binding of SARS-CoV S^B to hACE2 are labeled with a star. See also Data S1.

the SARS-CoV-2 S ectodomain trimer and reveal that it adopts multiple S^B conformations that are reminiscent of previous reports on both SARS-CoV S and MERS-CoV S. Finally, we show that SARS-CoV S mouse polyclonal sera potently inhibited entry into target cells of SARS-CoV-2 S pseudotyped viruses. Collectively, these results pave the way for designing vaccines eliciting broad protection against SARS-CoV-2, SARS-CoV, and SARSr-CoV.

RESULTS

ACE2 Is an Entry Receptor for SARS-CoV-2

The SARS-CoV-2 S glycoprotein shares 76% amino acid sequence identity with the SARS-CoV S Urbani and 80% identity with bat SARSr-CoV ZXC21 S and ZC45 S glycoprotein. The latter two SARSr-CoV sequences were identified from *Rinolophus sinicus* (Chinese horseshoe bats), the species from which SARSr-CoV WIV-1 and WIV-16 were isolated (Ge et al., 2013; Yang et al., 2015a). Furthermore, Zhou et al. (2020) recently reported that SARS-CoV-2 is most closely related to the bat SARSr-CoV RaTG13, with which it forms a distinct lineage from other SARSr-CoVs, and that their S glycoproteins share 97% amino acid sequence identity. SARS-CoV recognizes its entry receptor hACE2 at the surface of type II pneumocytes using S^B, which shares ~75% overall amino acid sequence identity with SARS-CoV-2 S^B and 50% identity within their receptor-binding motifs (RBMs) (Li et al., 2005a; Li et al., 2003; Li et al., 2005c; Wan et al., 2020). Previous studies also showed that the host proteases cathepsin L and TMPRSS2 prime SARS-CoV S for membrane fusion through cleavage at the S_1/S_2 and at the S_2' sites (Belouzard et al., 2009; Bosch et al., 2008; Glowacka et al., 2011; Matsuyama et al., 2010; Millet and Whittaker, 2015; Shulla et al., 2011).

We set out to investigate the functional determinants of S-mediated entry into target cells using a murine leukemia virus (MLV) pseudotyping system (Millet and Whittaker, 2016). To assess the ability of SARS-CoV-2 S to promote entry into target cells, we first compared transduction of SARS-CoV-2 S-MLV and SARS-CoV S-MLV into VeroE6 cells, that are known to express ACE2 and support SARS-CoV replication (Drosten et al., 2003; Ksiazek et al., 2003). Both pseudoviruses entered cells equally well (Figure 1A), suggesting that SARS-CoV-2 S-MLV could use African green monkey ACE2 as entry receptor. To confirm these results, we evaluated entry into BHK cells and observed that transient transfection with hACE2 rendered them susceptible to transduction with SARS-CoV-2 S-MLV (Figure 1B). These results demonstrate hACE2 is a functional receptor for SARS-CoV-2, in agreement with recently reported

Table 1. Kinetic Analysis of hACE2 Binding to SARS-CoV-2 S^B and SARS-CoV S^B by Biolayer Interferometry

	SARS-CoV-2 S^B	SARS-CoV S^B
K_D (nM)	1.2 ± 0.1	5.0 ± 0.1
k_{on} ($M^{-1}.s^{-1}$)	1.4×10^5 ($2.3 \pm 1.4 \times 10^5$)	1.4×10^5 ($1.7 \pm 0.7 \times 10^5$)
k_{off} (s^{-1})	1.6×10^{-4} ($1.7 \pm 0.8 \times 10^{-4}$)	$7.1x\ 10^{-4}$ ($8.7 \pm 5.1 \times 10^{-4}$)

Values reported represent the global fit to the data shown in Figures 2A and 2B and the averages obtained from five (SARS-CoV-2) or four (SARS-CoV) replicates carried out with different protein preparations are shown in parentheses.

findings (Hoffmann et al., 2020; Letko et al., 2020; Zhou et al., 2020).

Sequence analysis of SARS-CoV-2 S reveals the presence of a four amino acid residue insertion at the boundary between the S_1 and S_2 subunits compared with SARS-CoV S and SARSr-CoV S (Figure 1C). This results in the introduction of a furin cleavage site, a feature conserved among the 144 SARS-CoV-2 isolates sequenced to date but not in the closely related RaTG13 S (Zhou et al., 2020). Using western blot analysis, we observed that SARS-CoV-2 S was virtually entirely processed at the S_1/S_2 site during biosynthesis in HEK293T cells, presumably by furin in the Golgi compartment (Figure 1D). This observation contrasts with SARS-CoV S, which was incorporated into pseudovirions largely uncleaved (Figure 1D). To study the influence on pseudovirus entry of the SARS-CoV-2 S_1/S_2 furin cleavage site, we designed an S mutant lacking the four amino acid residue insertion and the furin cleavage site by mutating Q_{677}**TNSPRR**AR↓SV_{687} (wild-type SARS-CoV-2 S) to Q_{677}**TIL**R↓SV_{683} (SARS-CoV-2 $S_{fur/mut}$). SARS-CoV-2 $S_{fur/mut}$ preserves only the conserved arginine residue at position 685 of wild-type SARS-CoV-2 S, thereby mimicking the S_1/S_2 cleavage site of the related SARSr-CoV S CZX21 (Figure 1D). SARS-CoV-2 $S_{fur/mut}$ is therefore expected to undergo processing at the S_1/S_2 site upon encountering a target cell, similar to SARS-CoV S and SARSr-CoV S, i.e., via TMPRSS2 and/or cathepsin L (Belouzard et al., 2009; Bosch et al., 2008; Glowacka et al., 2011; Matsuyama et al., 2010; Millet and Whittaker, 2015; Shulla et al., 2011). As expected, SARS-CoV-2 $S_{fur/mut}$-MLV harbored uncleaved S upon budding (Figure 1D). The observed transduction efficiency of VeroE6 cells was higher for SARS-CoV-2 $S_{fur/mut}$-MLV than for SARS-CoV-2 S-MLV (Figure 1A), whereas the opposite trend was observed for transduction of hACE2-expressing BHK cells (Figure 1B). These results suggest that S_1/S_2 cleavage during S biosynthesis was not necessary for S-mediated entry in the conditions of our experiments (Figures 1C and 1D). We speculate that the detection of a polybasic cleavage site in the fusion glycoprotein of SARS-CoV-2 could putatively expand its tropism and/or enhance its transmissibility, compared with SARS-CoV and SARSr-CoV isolates, due to the near-ubiquitous distribution of furin-like proteases and their reported effects on other viruses (Klenk and Garten, 1994; Millet and Whittaker, 2015; Steinhauer, 1999).

SARS-CoV-2 Recognizes hACE2 with Comparable Affinity to SARS-CoV

The binding affinity of SARS-CoV for hACE2 correlates with the overall rate of viral replication in distinct species as well as with transmissibility and disease severity (Guan et al., 2003; Li et al., 2004; Li et al., 2005c; Wan et al., 2020). Indeed, specific S^B mutations enabled efficient binding to hACE2 of SARS-CoV isolates from the three phases of the 2002–2003 epidemic, which were associated with marked disease severity (Consortium, 2004; Kan et al., 2005; Li et al., 2005c; Sui et al., 2004). In contrast, SARS-CoV isolates detected during the brief 2003–2004 re-emergence interacted more weakly with hACE2 and had low pathogenicity and transmissibility (Consortium, 2004; Kan et al., 2005; Li et al., 2005c).

To understand the contribution of receptor interaction to the infectivity of SARS-CoV-2, we characterized engagement of hACE2 by SARS-CoV-2 S^B and SARS-CoV S^B side-by-side. We used biolayer interferometry to study binding kinetics and affinity of the purified hACE2 ectodomain to SARS-CoV-2 S^B and SARS-CoV S^B immobilized at the surface of biosensors. We found that hACE2 bound to SARS-CoV-2 S^B and SARS-CoV S^B with respective equilibrium dissociation constants of 1.2 nM (Figure 2A) and 5.0 nM (Figure 2B), and comparable kinetic rate constants, although the off-rate, were slightly higher for SARS-CoV S^B (Table 1). The affinity determined here for SARS-CoV S^B binding to hACE2 is in line with prior studies and the tighter apparent interactions formed by SARS-CoV S^B compared with the SARS-CoV S_1 subunit or the SARS-CoV S trimer (Kirchdoerfer et al., 2018; Li et al., 2005c; Sui et al., 2004; Walls et al., 2019; Wong et al., 2004). Previous structural work identified 14 positions that are key for binding of SARS-CoV S^B to hACE2: T402, R426, Y436, Y440, Y442, L472, N473, Y475, N479, Y484, T486, T487, G488, and Y491 (Li et al., 2005a). Analysis of the 144 SARS-CoV-2 genome sequences available from the Global Initiative on Sharing All Influenza Data (GISAID) (Elbe and Buckland-Merrett, 2017) shows that 8 out of these 14 positions are strictly conserved in SARS-CoV-2 S^B, whereas the other 6 positions are (semi)conservatively substituted: $R426_{SARS\text{-}CoV}N439_{SARS\text{-}CoV\text{-}2}$, $Y442_{SARS\text{-}CoV}L455_{SARS\text{-}CoV\text{-}2}$, $L472_{SARS\text{-}CoV}F486_{SARS\text{-}CoV\text{-}2}$, $N479_{SARS\text{-}CoV}Q493_{SARS\text{-}CoV\text{-}2}$, $Y484_{SARS\text{-}CoV}Q498_{SARS\text{-}CoV\text{-}2}$, and $T487_{SARS\text{-}CoV}N501_{SARS\text{-}CoV\text{-}2}$ (Figure 2C). The conservation of many key contact residues could explain the similar binding affinities of SARS-CoV-2 S^B and SARS-CoV S^B for hACE2. No mutations of residues predicted to contact hACE2 have been observed among SARS-CoV-2 S sequences available to date. However, we note that SARSr-CoV ZXC21 and ZC45, which harbor the most closely related S sequences after SARSr-CoV RaTG13, have a deletion in the RBD that could affect binding to hACE2 (between SARS-CoV-2 S residues 473–486) (Data S1). Collectively, these results suggest that SARS-CoV-2 is at least as well adapted to the

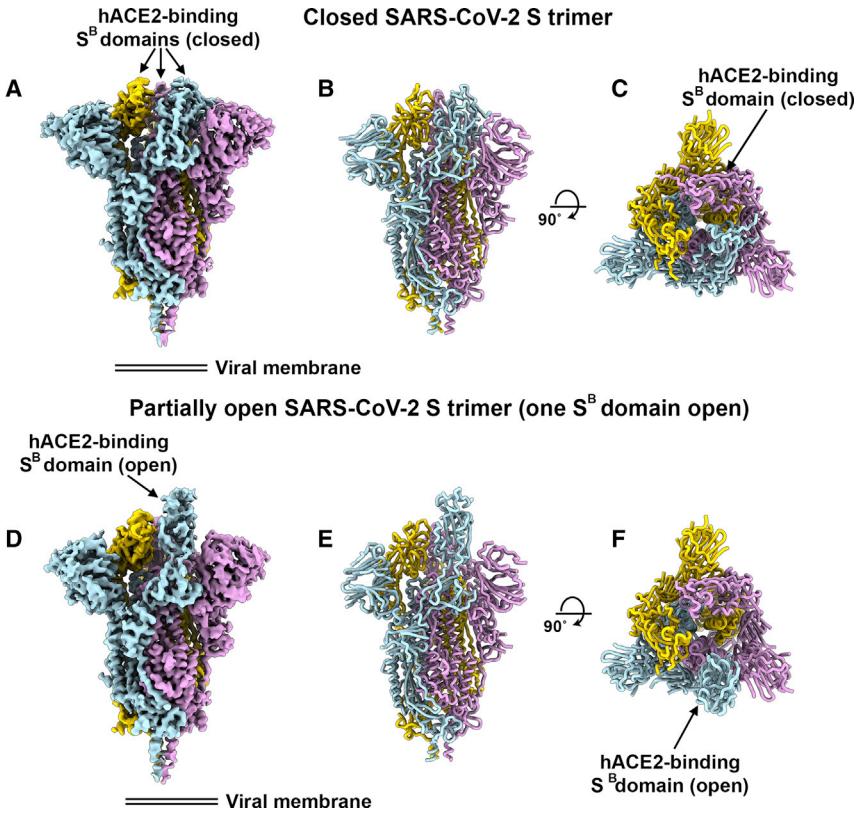

Figure 3. Cryo-EM Structures of the SARS-CoV-2 S Glycoprotein

(A) Closed SARS-CoV-2 S trimer unsharpened cryo-EM map.

(B and C) Two orthogonal views from the side (B) and top (C) of the atomic model of the closed SARS-CoV-2 S trimer.

(D) Partially open SARS-CoV-2 S trimer unsharpened cryo-EM map (one S^B domain is open).

(E-F) Two orthogonal views from the side (E) and top (F) of the atomic model of the closed SARS-CoV-2 S trimer. The glycans were omitted for clarity. See also Figures S1 and S2.

hACE2 ortholog as the 2002–2003 epidemic strains of SARS-CoV, which could explain the efficient transduction efficiency mediated by their respective S glycoproteins (Figures 1A and 1B) and the current rapid SARS-CoV-2 transmission in humans.

Architecture of the SARS-CoV-2 S Glycoprotein Trimer

To enable single-particle cryo-EM study of the SARS-CoV-2 S glycoprotein, we designed a prefusion stabilized ectodomain trimer construct with an abrogated furin S_1/S_2 cleavage site (Tortorici et al., 2019; Walls et al., 2017a; Walls et al., 2016a; Walls et al., 2019), two consecutive proline stabilizing mutations (Kirchdoerfer et al., 2018; Pallesen et al., 2017), and a C-terminal foldon trimerization domain (Miroshnikov et al., 1998). Three-dimensional (3D) classification of the cryo-EM data revealed the presence of multiple conformational states of SARS-CoV-2 S corresponding to distinct organization of the S^B domains within the S_1 apex. Approximately half of the particle images selected correspond to trimers harboring a single S^B domain opened whereas the remaining half was accounted for by closed trimers with the three S^B domains closed. A recently determined SARS-CoV-2 S structure also detected trimers with a single S^B domain opened but none entirely closed (Wrapp et al., 2020). The observed conformational variability of S^B domains is reminiscent of observations made with SARS-CoV S and MERS-CoV S trimers, although we did not detect trimers with two S^B domains open and the distribution of particles across the S conformational landscape varies among studies (Gui et al., 2017; Kirchdoerfer et al., 2018; Pallesen et al., 2017; Song et al., 2018; Walls et al., 2019; Yuan et al., 2017).

We determined a reconstruction of the closed SARS-CoV-2 S ectodomain trimer at 2.8 Å resolution (applying 3-fold symmetry) and an asymmetric reconstruction of the trimer with a single S^B domain opened at 3.2 Å resolution (Figures 3A–3H and S1; Table S1). The S_2 fusion machinery is the best resolved part of the map, whereas the S^A and S^B domains are less well resolved, presumably because of conformational heterogeneity. The atomic model comprises residues 27-1147, with internal breaks corresponding to flexible regions (including part of the RBM), and lacks the C-terminal most segment (including the heptad repeat 2) that is not visible in the map, as is the case for all S structures determined to date. Overall, the SARS-CoV-2 S ectodomain is a 160-Å-long trimer with a triangular cross-section, resembling the closely related SARS-CoV S structure (Figures S2A–S2F) (Gui et al., 2017; Kirchdoerfer et al., 2018; Song et al., 2018; Walls et al., 2019; Yuan et al., 2017).

As is the case for other β-coronavirus S glycoproteins, including SARS-CoV S (Gui et al., 2017; Kirchdoerfer et al., 2018; Pallesen et al., 2017; Park et al., 2019; Song et al., 2018; Tortorici et al., 2019; Walls et al., 2016a; Walls et al., 2016b; Walls et al., 2019; Yuan et al., 2017), the S_1 subunit has a V-shaped architecture (Figures S2B–S2E). In the closed S trimer, the three hACE2-recognition motifs, whose location was inferred based on the crystal structure of SARS-CoV S^B in complex with hACE2 (Li et al., 2005a), are buried at the interface between protomers. As a result, SARS-CoV-2 S^B opening is expected to be necessary for interacting with ACE2 at the host cell surface and initiating the conformational changes leading to cleavage of the S_2' site, membrane fusion and viral entry (Gui et al., 2017; Kirchdoerfer et al., 2018; Millet and Whittaker, 2014; Pallesen et al., 2017; Park et al., 2016; Song et al., 2018; Walls et al., 2019; Yuan et al., 2017).

As the SARS-CoV-2 and SARS-CoV S_2 subunits share 88% sequence identity, they are structurally conserved and can be superimposed with 1.2 Å root-mean-square deviation (rmsd) over 417 aligned Cα positions (Figures S2E and S2F). Only the most N-terminal part of the fusion peptide is resolved in the map, as was the case for previously determined SARS-CoV S

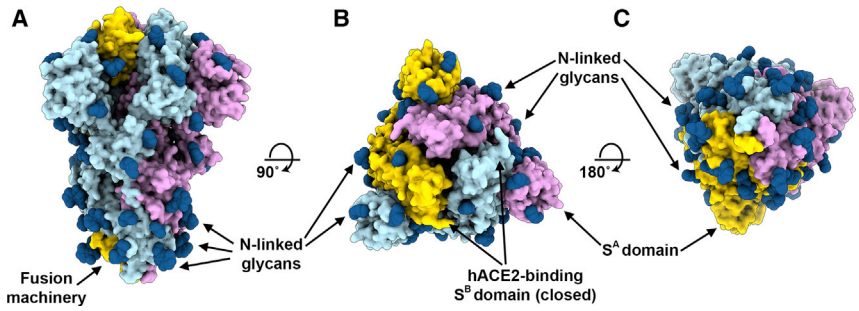

Figure 4. Organization of the SARS-CoV-2 S N-Linked Glycans

(A–C) Ribbon diagrams of the SARS-CoV-2 S closed structure rendered as a surface with glycans resolved in the cryo-EM map rendered as dark blue spheres. See also Table 2 and Data S1.

structures. The sequence and conformational conservation of the fusion peptide region observed across SARS-CoV-2 S and SARS-CoV S suggests that Abs targeting this functionally important motif might cross-react and neutralize the two viruses as well as related coronaviruses.

We previously showed that coronavirus S glycoproteins are densely decorated by heterogeneous N-linked glycans protruding from the trimer surface (Walls et al., 2016b; Walls et al., 2019; Xiong et al., 2018). These oligosaccharides participate in S folding (Rossen et al., 1998), affect priming by host proteases (Yang et al., 2015b), and might modulate antibody recognition (Pallesen et al., 2017; Walls et al., 2019). SARS-CoV-2 S comprise 22 N-linked glycosylation sequons per protomer and oligosaccharides are resolved in the cryo-EM map for 16 of these sites (Figure 4). By comparison, SARS-CoV S possesses 23 N-linked glycosylation sequons per protomer, and we previously experimentally confirmed that at least 19 of them are glycosylated (Walls et al., 2019). 20 out of 22 SARS-CoV-2 S N-linked glycosylation sequons are conserved in SARS-CoV S (Table 2). Specifically, 9 out of 13 glycans in the S_1 subunit and all 9 glycans in the S_2 subunit are conserved among SARS-CoV-2 S and SARS-CoV S. Furthermore, S_2 N-linked glycosylation sequons are mostly conserved across SARSr-CoV S glycoproteins, suggesting that accessibility of the fusion machinery to Abs will be comparable among these viruses (Table 2 and Data S1).

SARS-CoV S Elicits Neutralizing Abs Against SARS-CoV-2 S

Mapping of the sequence conservation across multiple S sequences from the sarbecovirus subgenus underscores that the S_2 fusion machinery is more conserved than the S_1 subunit with the highest divergence found within S^A and S^B (Figures 5A and 5B). These observations are in line with (1) the fact that some, but not all, of these viruses use ACE2 as entry receptor (Ge et al., 2013; Ren et al., 2008; Yang et al., 2015a); and (2) that the S_1 subunit is more exposed at the viral surface than the fusion machinery and is likely to be subject to a more stringent selection pressure from the immune system.

Based on these observations, we hypothesized that exposure to one of the two viruses could elicit cross-reactive and potentially neutralizing Abs against the other virus. We therefore investigated the ability of plasma from four mice immunized with a stabilized SARS-CoV S to inhibit SARS-CoV-2 S- and SARS-CoV S-mediated entry into target cells. All sera tested completely inhibited transduction of SARS-CoV S-MLV and reduced SARS-CoV-2 S-MLV transduction to ~10% of control in VeroE6 cells (Figure 5C). The elicitation of a heterotypic response blocking SARS-CoV-2 S-mediated entry into host cells concurs with the sequence and structural conservation of SARS-CoV-2 S and SARS-CoV S along with their comparable glycans shields and suggests that immunity against one virus of the sarbecovirus subgenus can potentially provide protection against related viruses.

DISCUSSION

Receptor recognition is the first step of viral infection and is a key determinant of host cell and tissue tropism. Enhanced binding affinity between SARS-CoV S and hACE2 was proposed to correlate with increased virus transmissibility and disease severity in humans (Li et al., 2005c). Indeed, SARS-CoV isolates from the three phases of the 2002–2003 epidemic were more efficiently transmitted among humans and more pathogenic than the isolates associated with the 2003–2004 re-emergence that caused only a few cases, in line with their binding affinities for hACE2 (Consortium, 2004; Kan et al., 2005; Li et al., 2005c). Moreover, the ability to engage ACE2 from different animal species appears to reflect host susceptibility to SARS-CoV infection and facilitated the jump of the virus from animals to humans (Li, 2008; Li et al., 2004). We report here that SARS-CoV-2 uses hACE2 as an entry receptor and recognizes it with a similar affinity to the 2002–2003 SARS-CoV isolates, which suggests it can spread efficiently in humans, in agreement with the numerous SARS-CoV-2 human-to-human transmission events reported to date.

Besides binding to host cell receptors, priming of the S glycoprotein by host proteases through cleavage at the S_1/S_2 and the S_2' sites is another crucial factor modulating tropism and pathogenicity (Millet and Whittaker, 2015). For instance, entry of the MERS-CoV-related bat coronavirus HKU4 into human cells required addition of exogenous trypsin, indicating that S proteolytic activation of this bat virus did not occur in human cells (despite its ability to recognize human DPP4) (Wang et al., 2014; Yang et al., 2014). Subsequent work suggested that a glycan present near the S_1/S_2 boundary accounted for the lack of proteolytic priming of HKU4 S and that its removal enhanced pseudovirus entry in human cells (Yang et al., 2015b). The presence of a polybasic cleavage site, that can be processed by furin-like proteases, is a signature of several highly pathogenic avian influenza viruses and

Table 2. Conservation of N-Linked Glycosylation Sequons in SARS-CoV-2 S and SARS-CoV S

SARS-CoV-2 S	SARS-CoV S
N_{17}LT	*T_{21}FD*
P_{25}PA	N_{29}YT
N_{61}VT	N_{65}VT
H_{69}VS	N_{73}HT
N_{74}GT	. . .
S_{112}KT	N_{109}KS
N_{121}NA	N_{118}NS
N_{122}AT	N_{119}ST
N_{149}KS	*T_{146}QT*
N_{165}CT	N_{158}CT
N_{234}IT	N_{227}IT
N_{282}GT	N_{269}GT
N_{331}IT	N_{318}IT
N_{343}AT	N_{330}AT
N_{370}SA	N_{357}ST
N_{603}TS	N_{589}AS
N_{616}CT	N_{602}CT
N_{657}NS	*D_{643}TS*
N_{709}NS	N_{691}NT
N_{717}FT	N_{699}FS
N_{801}FS	N_{783}FS
N_{1074}FT	N_{1056}FT
N_{1098}GT	N_{1080}GT
N_{1134}NT	N_{1116}NT
N_{1158}HT	N_{1140}HT
N_{1173}AS	N_{1155}AS
N_{1194}ES	N_{1176}ES

Italic font indicates the absence of a glycosylation sequon and deletions are indicated with periods. Glycans observed in the SARS-CoV-2 S cryo-EM map are underlined. See also Data S1.

pathogenic Newcastle disease virus (Klenk and Garten, 1994; Steinhauer, 1999). Strikingly, SARS-CoV-2 S harbors a furin cleavage site at the S_1/S_2 boundary, which is processed during biosynthesis. The presence of a furin cleavage site sets SARS-CoV-2 S apart from SARS-CoV S (and SARSr-CoV S) that possesses a monobasic S_1/S_2 cleavage site processed upon entry of target cells (Belouzard et al., 2009; Bosch et al., 2008; Glowacka et al., 2011; Matsuyama et al., 2010; Millet and Whittaker, 2015; Shulla et al., 2011). We speculate that the almost ubiquitous expression of furin-like proteases could participate in expanding SARS-CoV-2 cell and tissue tropism, relative to SARS-CoV, as well as increasing its transmissibility and/or altering its pathogenicity.

We previously suggested that coronaviruses use conformational masking and glycan shielding to limit recognition by the immune response of infected hosts (Walls et al., 2016b; Walls et al., 2019; Xiong et al., 2018). Similarly to SARS-CoV S and MERS-CoV S (Gui et al., 2017; Kirchdoerfer et al., 2018; Pallesen et al., 2017; Song et al., 2018; Walls et al., 2019; Yuan et al., 2017), we found that the SARS-CoV-2 S trimer exists in multiple, distinct conformational states resulting from S^B opening at the trimer apex. These structural changes are necessary for receptor engagement of these three viruses and lead to initiation of fusogenic conformational changes (Song et al., 2018; Walls et al., 2017b; Walls et al., 2019). In contrast, only closed S trimers have been detected for the four other human-infecting coronaviruses: HCoV-NL63 (Walls et al., 2016b), HCoV-OC43 (Tortorici et al., 2019), HCoV-HKU1 (Kirchdoerfer et al., 2016), and HCoV-229E (Li et al., 2019). As HCoV-NL63 and HCoV-229E are known to engage protein receptors through S^B (Wong et al., 2017; Wu et al., 2009), trimer opening is also expected to occur to expose their RBMs that are otherwise buried at the interface between protomers in the closed S trimers (Li et al., 2019; Walls et al., 2016b). Regardless of the nature of the receptor and the location of the receptor-binding domains, removal of the trimeric S_1 crown is expected to be necessary for all coronaviruses to allow the large-scale S_2 conformational changes leading to fusion of the viral and host membranes (Walls et al., 2017b). Collectively, these data underscore that S glycoprotein trimers found in highly pathogenic human coronaviruses appear to exist in partially opened states, while they remain largely closed in human coronaviruses associated with common colds. Based on the aforementioned data correlating the binding affinity of SARS-CoV for hACE2 with the rate of transmissibility, viral replication in distinct species, and disease severity (Guan et al., 2003; Li et al., 2004; Li et al., 2005c; Wan et al., 2020), we hypothesize that the most pathogenic coronaviruses will exhibit S glycoprotein trimers spontaneously sampling closed and open conformations, as is the case for SARS-CoV-2, SARS-CoV and MERS-CoV.

The striking structural similarity and sequence conservation among the SARS-CoV-2 S and SARS-CoV S glycoproteins emphasize the close relationship between these two viruses that recognize hACE2 to enter target cells. This resemblance is further strengthened by our finding that SARS-CoV S elicited polyclonal Ab responses, potently neutralizing SARS-CoV-2 S-mediated entry into cells. We surmise most of these Abs target the highly conserved S_2 subunit (including the fusion peptide region) based on its structural similarity across SARS-CoV-2 and SARS-CoV, the lack of cross-reactivity of several S^B-directed Abs (Tian et al., 2020; Wrapp et al., 2020), and previous reports showing that sera from SARS-CoV-infected individuals target this region (Zhang et al., 2004). We note that most SARS-CoV neutralizing Abs isolated to date target the S^B domain and that several of them recognize the RBM and prevent receptor engagement (Hwang et al., 2006; Rockx et al., 2008; Rockx et al., 2010; Traggiai et al., 2004; Walls et al., 2019). As the SARS-CoV-2 and SARS-CoV S^B domains share 75% amino acid sequence identity, future work will be necessary to evaluate whether any of these Abs neutralize the newly emerged coronavirus. These findings also indicate that it might be difficult to distinguish exposure to SARS-CoV-2 from other SARSr-CoVs in serological studies using S ectodomain trimers and that specific assays will need to be designed. Our results provide a structural framework to identify conserved and accessible epitopes across S glycoproteins that will support

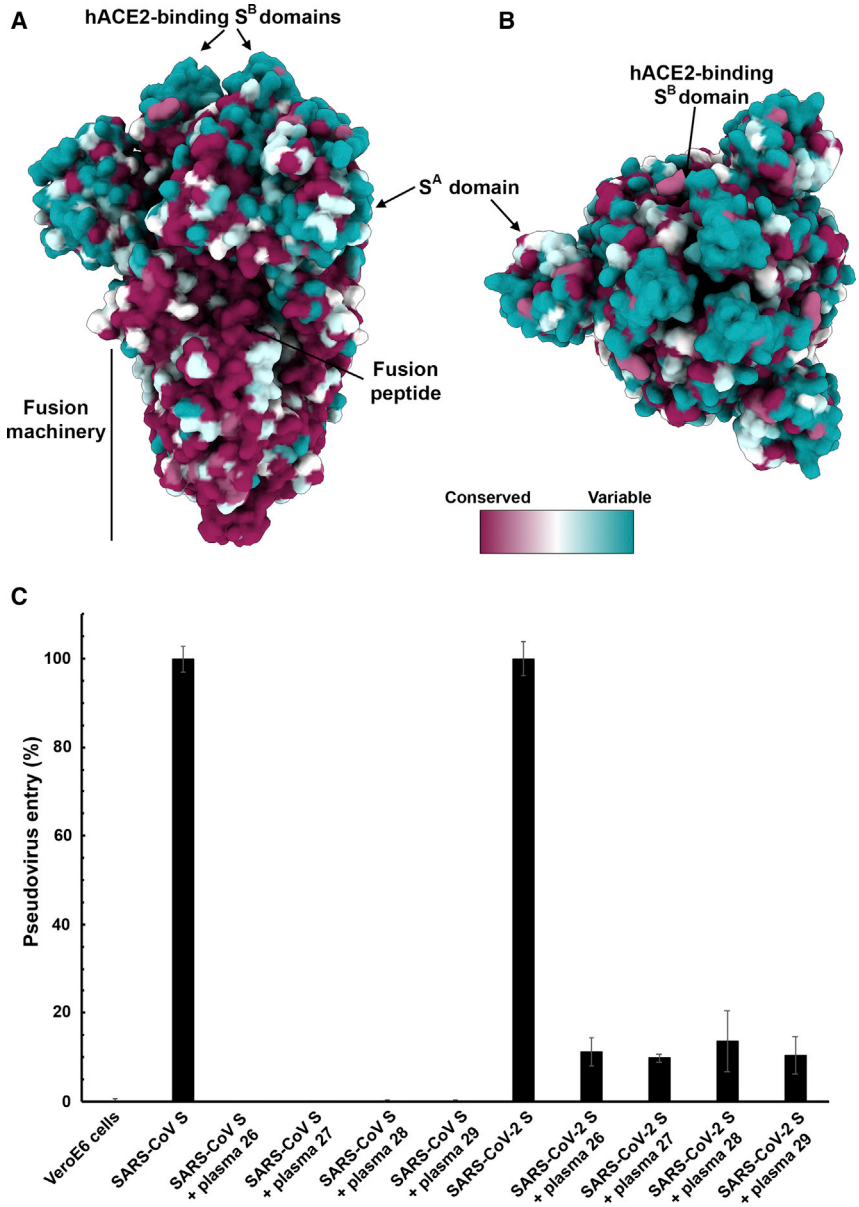

Figure 5. SARS-CoV S Elicits Antibodies Neutralizing SARS-CoV-2 S-Mediated Entry into Host Cells

(A and B) Sequence conservation of sarbecovirus S glycoproteins plotted on the SARS-CoV-2 S structure viewed from the side (A) and top (B). The sequence alignment was generated using 48 SARS-CoV-2 S sequences obtained from GISAID in addition to the sequences listed in Data S1.

(C) Entry of SARS-CoV-2 S-MLV and SARS-CoV S-MLV is potently inhibited by four SARS-CoV S mouse polyclonal immune plasma.

ongoing vaccine design efforts. Finally, elicitation of diverse, polyclonal Ab responses might prove key in light of the diversity of viruses circulating in animal reservoirs and in preventing the possible emergence of viral neutralization escape mutants.

STAR★METHODS

Detailed methods are provided in the online version of this paper and include the following:

- KEY RESOURCES TABLE
- LEAD CONTACT AND MATERIALS AVAILABILITY
- EXPERIMENTAL MODEL AND SUBJECT DETAILS
  - Cell lines
- METHOD DETAILS
  - Transient expression of SARS-CoV-2 and SARS-CoV S^B
  - Transient expression of hACE2
  - Pseudovirus production
  - Western Blotting
  - Pseudovirus entry assays
  - Biolayer interferometry
  - Protein expression and purification
  - CryoEM sample preparation and data collection
  - Cryo-EM data processing
  - CryoEM model building and analysis
  - Immunizations with SARS-CoV S
- QUANTIFICATION AND STATISTICAL ANALYSIS
- DATA AND CODE AVAILABILITY

SUPPLEMENTAL INFORMATION

Supplemental Information can be found online at https://doi.org/10.1016/j.cell.2020.02.058.

ACKNOWLEDGMENTS

This study was supported by the National Institute of General Medical Sciences (R01GM120553 to D.V.), the National Institute of Allergy and Infectious Diseases (HHSN272201700059C to D.V.), a Pew Biomedical Scholars Award (D.V.), an Investigators in the Pathogenesis of Infectious Disease Award from the Burroughs Wellcome Fund (D.V.), the University of Washington Arnold and Mabel Beckman cryoEM center, the Washington Research Foundation, and the Pasteur Institute (M.A.T.). We are grateful to Lynda Stuart for sharing the full-length hACE2 plasmid, to Gary Whittaker for the MLV pseudotyping system, and to Ning Zheng for providing access to the Octet device.

AUTHOR CONTRIBUTIONS

A.C.W., Y.-J.P., A.T.M., and D.V. designed the experiments. A.C.W. and M.A.T. expressed and purified the proteins. A.C.W. carried out binding assays and pseudovirus entry assays. Y.-J.P. prepared samples for cryo-EM and collected the data. Y.-J.P. and D.V. processed the data and built and refined the atomic models. A.W. and A.T.M. immunized mice. A.C.W., Y.-J.P., and D.V. analyzed the data and prepared the manuscript with input from all authors.

DECLARATION OF INTERESTS

The authors declare no competing financial interests.

Received: February 19, 2020
Revised: February 24, 2020
Accepted: February 26, 2020
Published: March 9, 2020

REFERENCES

Agirre, J., Iglesias-Fernández, J., Rovira, C., Davies, G.J., Wilson, K.S., and Cowtan, K.D. (2015). Privateer: software for the conformational validation of carbohydrate structures. Nat. Struct. Mol. Biol. *22*, 833–834.

Anthony, S.J., Gilardi, K., Menachery, V.D., Goldstein, T., Ssebide, B., Mbabazi, R., Navarrete-Macias, I., Liang, E., Wells, H., Hicks, A., et al. (2017). Further Evidence for Bats as the Evolutionary Source of Middle East Respiratory Syndrome Coronavirus. MBio *8*, e00373-17.

Ashkenazy, H., Abadi, S., Martz, E., Chay, O., Mayrose, I., Pupko, T., and Ben-Tal, N. (2016). ConSurf 2016: an improved methodology to estimate and visualize evolutionary conservation in macromolecules. Nucleic Acids Res. *44*, W344-50.

Barad, B.A., Echols, N., Wang, R.Y., Cheng, Y., DiMaio, F., Adams, P.D., and Fraser, J.S. (2015). EMRinger: side chain-directed model and map validation for 3D cryo-electron microscopy. Nat. Methods *12*, 943–946.

Belouzard, S., Chu, V.C., and Whittaker, G.R. (2009). Activation of the SARS coronavirus spike protein via sequential proteolytic cleavage at two distinct sites. Proc. Natl. Acad. Sci. USA *106*, 5871–5876.

Bosch, B.J., van der Zee, R., de Haan, C.A., and Rottier, P.J. (2003). The coronavirus spike protein is a class I virus fusion protein: structural and functional characterization of the fusion core complex. J. Virol. *77*, 8801–8811.

Bosch, B.J., Bartelink, W., and Rottier, P.J. (2008). Cathepsin L functionally cleaves the severe acute respiratory syndrome coronavirus class I fusion protein upstream of rather than adjacent to the fusion peptide. J. Virol. *82*, 8887–8890.

Brown, A., Long, F., Nicholls, R.A., Toots, J., Emsley, P., and Murshudov, G. (2015). Tools for macromolecular model building and refinement into electron cryo-microscopy reconstructions. Acta Crystallogr. D Biol. Crystallogr. *71*, 136–153.

Burkard, C., Verheije, M.H., Wicht, O., van Kasteren, S.I., van Kuppeveld, F.J., Haagmans, B.L., Pelkmans, L., Rottier, P.J., Bosch, B.J., and de Haan, C.A. (2014). Coronavirus cell entry occurs through the endo-/lysosomal pathway in a proteolysis-dependent manner. PLoS Pathog. *10*, e1004502.

Chen, V.B., Arendall, W.B., 3rd, Headd, J.J., Keedy, D.A., Immormino, R.M., Kapral, G.J., Murray, L.W., Richardson, J.S., and Richardson, D.C. (2010). MolProbity: all-atom structure validation for macromolecular crystallography. Acta Crystallogr. D Biol. Crystallogr. *66*, 12–21.

Consortium, C.S.M.E.; Chinese SARS Molecular Epidemiology Consortium (2004). Molecular evolution of the SARS coronavirus during the course of the SARS epidemic in China. Science *303*, 1666–1669.

Corti, D., Zhao, J., Pedotti, M., Simonelli, L., Agnihothram, S., Fett, C., Fernandez-Rodriguez, B., Foglierini, M., Agatic, G., Vanzetta, F., et al. (2015). Prophylactic and postexposure efficacy of a potent human monoclonal antibody against MERS coronavirus. Proc. Natl. Acad. Sci. USA *112*, 10473–10478.

Drosten, C., Günther, S., Preiser, W., van der Werf, S., Brodt, H.R., Becker, S., Rabenau, H., Panning, M., Kolesnikova, L., Fouchier, R.A., et al. (2003). Identification of a novel coronavirus in patients with severe acute respiratory syndrome. N. Engl. J. Med. *348*, 1967–1976.

Elbe, S., and Buckland-Merrett, G. (2017). Data, disease and diplomacy: GISAID's innovative contribution to global health. Glob Chall. *1*, 33–46.

Emsley, P., Lohkamp, B., Scott, W.G., and Cowtan, K. (2010). Features and development of Coot. Acta Crystallogr. D Biol. Crystallogr. *66*, 486–501.

Frenz, B., Rämisch, S., Borst, A.J., Walls, A.C., Adolf-Bryfogle, J., Schief, W.R., Veesler, D., and DiMaio, F. (2019). Automatically fixing errors in glycoprotein structures with Rosetta. Structure *27*, 134–139.e3.

Ge, X.Y., Li, J.L., Yang, X.L., Chmura, A.A., Zhu, G., Epstein, J.H., Mazet, J.K., Hu, B., Zhang, W., Peng, C., et al. (2013). Isolation and characterization of a bat SARS-like coronavirus that uses the ACE2 receptor. Nature *503*, 535–538.

Glowacka, I., Bertram, S., Müller, M.A., Allen, P., Soilleux, E., Pfefferle, S., Steffen, I., Tsegaye, T.S., He, Y., Gnirss, K., et al. (2011). Evidence that TMPRSS2 activates the severe acute respiratory syndrome coronavirus spike protein for membrane fusion and reduces viral control by the humoral immune response. J. Virol. *85*, 4122–4134.

Goddard, T.D., Huang, C.C., and Ferrin, T.E. (2007). Visualizing density maps with UCSF Chimera. J. Struct. Biol. *157*, 281–287.

Goddard, T.D., Huang, C.C., Meng, E.C., Pettersen, E.F., Couch, G.S., Morris, J.H., and Ferrin, T.E. (2018). UCSF ChimeraX: Meeting modern challenges in visualization and analysis. Protein Sci. *27*, 14–25.

Guan, Y., Zheng, B.J., He, Y.Q., Liu, X.L., Zhuang, Z.X., Cheung, C.L., Luo, S.W., Li, P.H., Zhang, L.J., Guan, Y.J., et al. (2003). Isolation and characterization of viruses related to the SARS coronavirus from animals in southern China. Science *302*, 276–278.

Gui, M., Song, W., Zhou, H., Xu, J., Chen, S., Xiang, Y., and Wang, X. (2017). Cryo-electron microscopy structures of the SARS-CoV spike glycoprotein reveal a prerequisite conformational state for receptor binding. Cell Res. *27*, 119–129.

Haagmans, B.L., Al Dhahiry, S.H., Reusken, C.B., Raj, V.S., Galiano, M., Myers, R., Godeke, G.J., Jonges, M., Farag, E., Diab, A., et al. (2014). Middle East respiratory syndrome coronavirus in dromedary camels: an outbreak investigation. Lancet Infect. Dis. *14*, 140–145.

Heald-Sargent, T., and Gallagher, T. (2012). Ready, set, fuse! The coronavirus spike protein and acquisition of fusion competence. Viruses *4*, 557–580.

Hoffmann, M., Kleine-Weber, H., Krüger, N., Müller, M., Drosten, C., and Pöhlmann, S. (2020). The novel coronavirus 2019 (2019-nCoV) uses the SARS-coronavirus receptor ACE2 and the cellular protease TMPRSS2

for entry into target cells. bioRxiv. https://doi.org/10.1101/2020.01.31.929042.

Hu, B., Zeng, L.P., Yang, X.L., Ge, X.Y., Zhang, W., Li, B., Xie, J.Z., Shen, X.R., Zhang, Y.Z., Wang, N., et al. (2017). Discovery of a rich gene pool of bat SARS-related coronaviruses provides new insights into the origin of SARS coronavirus. PLoS Pathog. *13*, e1006698.

Huang, C., Wang, Y., Li, X., Ren, L., Zhao, J., Hu, Y., Zhang, L., Fan, G., Xu, J., Gu, X., et al. (2020). Clinical features of patients infected with 2019 novel coronavirus in Wuhan (China: Lancet).

Hulswit, R.J.G., Lang, Y., Bakkers, M.J.G., Li, W., Li, Z., Schouten, A., Ophorst, B., van Kuppeveld, F.J.M., Boons, G.J., Bosch, B.J., et al. (2019). Human coronaviruses OC43 and HKU1 bind to 9-*O*-acetylated sialic acids via a conserved receptor-binding site in spike protein domain A. Proc. Natl. Acad. Sci. USA *116*, 2681–2690.

Hwang, W.C., Lin, Y., Santelli, E., Sui, J., Jaroszewski, L., Stec, B., Farzan, M., Marasco, W.A., and Liddington, R.C. (2006). Structural basis of neutralization by a human anti-severe acute respiratory syndrome spike protein antibody, 80R. J. Biol. Chem. *281*, 34610–34616.

Kan, B., Wang, M., Jing, H., Xu, H., Jiang, X., Yan, M., Liang, W., Zheng, H., Wan, K., Liu, Q., et al. (2005). Molecular evolution analysis and geographic investigation of severe acute respiratory syndrome coronavirus-like virus in palm civets at an animal market and on farms. J. Virol. *79*, 11892–11900.

Kirchdoerfer, R.N., Cottrell, C.A., Wang, N., Pallesen, J., Yassine, H.M., Turner, H.L., Corbett, K.S., Graham, B.S., McLellan, J.S., and Ward, A.B. (2016). Pre-fusion structure of a human coronavirus spike protein. Nature *531*, 118–121.

Kirchdoerfer, R.N., Wang, N., Pallesen, J., Wrapp, D., Turner, H.L., Cottrell, C.A., Corbett, K.S., Graham, B.S., McLellan, J.S., and Ward, A.B. (2018). Stabilized coronavirus spikes are resistant to conformational changes induced by receptor recognition or proteolysis. Sci. Rep. *8*, 15701.

Klenk, H.D., and Garten, W. (1994). Host cell proteases controlling virus pathogenicity. Trends Microbiol. *2*, 39–43.

Ksiazek, T.G., Erdman, D., Goldsmith, C.S., Zaki, S.R., Peret, T., Emery, S., Tong, S., Urbani, C., Comer, J.A., Lim, W., et al.; SARS Working Group (2003). A novel coronavirus associated with severe acute respiratory syndrome. N. Engl. J. Med. *348*, 1953–1966.

Letko, M., Marzi, A., and Munster, V. (2020). Functional assessment of cell entry and receptor usage for SARS-CoV-2 and other lineage B betacoronaviruses. Nat. Microbiol. Published online February 24, 2020. https://doi.org/10.1038/s41564-020-0688-y.

Li, F. (2008). Structural analysis of major species barriers between humans and palm civets for severe acute respiratory syndrome coronavirus infections. J. Virol. *82*, 6984–6991.

Li, W., Moore, M.J., Vasilieva, N., Sui, J., Wong, S.K., Berne, M.A., Somasundaran, M., Sullivan, J.L., Luzuriaga, K., Greenough, T.C., et al. (2003). Angiotensin-converting enzyme 2 is a functional receptor for the SARS coronavirus. Nature *426*, 450–454.

Li, W., Greenough, T.C., Moore, M.J., Vasilieva, N., Somasundaran, M., Sullivan, J.L., Farzan, M., and Choe, H. (2004). Efficient replication of severe acute respiratory syndrome coronavirus in mouse cells is limited by murine angiotensin-converting enzyme 2. J. Virol. *78*, 11429–11433.

Li, F., Li, W., Farzan, M., and Harrison, S.C. (2005a). Structure of SARS coronavirus spike receptor-binding domain complexed with receptor. Science *309*, 1864–1868.

Li, W., Shi, Z., Yu, M., Ren, W., Smith, C., Epstein, J.H., Wang, H., Crameri, G., Hu, Z., Zhang, H., et al. (2005b). Bats are natural reservoirs of SARS-like coronaviruses. Science *310*, 676–679.

Li, W., Zhang, C., Sui, J., Kuhn, J.H., Moore, M.J., Luo, S., Wong, S.K., Huang, I.C., Xu, K., Vasilieva, N., et al. (2005c). Receptor and viral determinants of SARS-coronavirus adaptation to human ACE2. EMBO J. *24*, 1634–1643.

Li, W., Hulswit, R.J.G., Widjaja, I., Raj, V.S., McBride, R., Peng, W., Widagdo, W., Tortorici, M.A., van Dieren, B., Lang, Y., et al. (2017). Identification of sialic acid-binding function for the Middle East respiratory syndrome coronavirus spike glycoprotein. Proc. Natl. Acad. Sci. USA *114*, E8508–E8517.

Li, Z., Tomlinson, A.C., Wong, A.H., Zhou, D., Desforges, M., Talbot, P.J., Benlekbir, S., Rubinstein, J.L., and Rini, J.M. (2019). The human coronavirus HCoV-229E S-protein structure and receptor binding. eLife *8*, e51230.

Liebschner, D., Afonine, P.V., Baker, M.L., Bunkóczi, G., Chen, V.B., Croll, T.I., Hintze, B., Hung, L.W., Jain, S., McCoy, A.J., et al. (2019). Macromolecular structure determination using X-rays, neutrons and electrons: recent developments in Phenix. Acta Crystallogr. D Struct. Biol. *75*, 861–877.

Lu, G., Hu, Y., Wang, Q., Qi, J., Gao, F., Li, Y., Zhang, Y., Zhang, W., Yuan, Y., Bao, J., et al. (2013). Molecular basis of binding between novel human coronavirus MERS-CoV and its receptor CD26. Nature *500*, 227–231.

Madu, I.G., Roth, S.L., Belouzard, S., and Whittaker, G.R. (2009). Characterization of a highly conserved domain within the severe acute respiratory syndrome coronavirus spike protein S2 domain with characteristics of a viral fusion peptide. J. Virol. *83*, 7411–7421.

Matsuyama, S., Nagata, N., Shirato, K., Kawase, M., Takeda, M., and Taguchi, F. (2010). Efficient activation of the severe acute respiratory syndrome coronavirus spike protein by the transmembrane protease TMPRSS2. J. Virol. *84*, 12658–12664.

Memish, Z.A., Mishra, N., Olival, K.J., Fagbo, S.F., Kapoor, V., Epstein, J.H., Alhakeem, R., Durosinloun, A., Al Asmari, M., Islam, A., et al. (2013). Middle East respiratory syndrome coronavirus in bats, Saudi Arabia. Emerg. Infect. Dis. *19*, 1819–1823.

Menachery, V.D., Yount, B.L., Jr., Debbink, K., Agnihothram, S., Gralinski, L.E., Plante, J.A., Graham, R.L., Scobey, T., Ge, X.Y., Donaldson, E.F., et al. (2015). A SARS-like cluster of circulating bat coronaviruses shows potential for human emergence. Nat. Med. *21*, 1508–1513.

Menachery, V.D., Yount, B.L., Jr., Sims, A.C., Debbink, K., Agnihothram, S.S., Gralinski, L.E., Graham, R.L., Scobey, T., Plante, J.A., Royal, S.R., et al. (2016). SARS-like WIV1-CoV poised for human emergence. Proc. Natl. Acad. Sci. USA *113*, 3048–3053.

Millet, J.K., and Whittaker, G.R. (2014). Host cell entry of Middle East respiratory syndrome coronavirus after two-step, furin-mediated activation of the spike protein. Proc. Natl. Acad. Sci. USA *111*, 15214–15219.

Millet, J.K., and Whittaker, G.R. (2015). Host cell proteases: Critical determinants of coronavirus tropism and pathogenesis. Virus Res. *202*, 120–134.

Millet, J.K., and Whittaker, G.R. (2016). Murine Leukemia Virus (MLV)-based Coronavirus Spike-pseudotyped Particle Production and Infection. Bio Protoc. *6*, e2035.

Miroshnikov, K.A., Marusich, E.I., Cerritelli, M.E., Cheng, N., Hyde, C.C., Steven, A.C., and Mesyanzhinov, V.V. (1998). Engineering trimeric fibrous proteins based on bacteriophage T4 adhesins. Protein Eng. *11*, 329–332.

Pallesen, J., Wang, N., Corbett, K.S., Wrapp, D., Kirchdoerfer, R.N., Turner, H.L., Cottrell, C.A., Becker, M.M., Wang, L., Shi, W., et al. (2017). Immunogenicity and structures of a rationally designed prefusion MERS-CoV spike antigen. Proc. Natl. Acad. Sci. USA *114*, E7348–E7357.

Park, J.E., Li, K., Barlan, A., Fehr, A.R., Perlman, S., McCray, P.B., Jr., and Gallagher, T. (2016). Proteolytic processing of Middle East respiratory syndrome coronavirus spikes expands virus tropism. Proc. Natl. Acad. Sci. USA *113*, 12262–12267.

Park, Y.J., Walls, A.C., Wang, Z., Sauer, M.M., Li, W., Tortorici, M.A., Bosch, B.J., DiMaio, F., and Veesler, D. (2019). Structures of MERS-CoV spike glycoprotein in complex with sialoside attachment receptors. Nat. Struct. Mol. Biol. *26*, 1151–1157.

Punjani, A., Rubinstein, J.L., Fleet, D.J., and Brubaker, M.A. (2017). cryoSPARC: algorithms for rapid unsupervised cryo-EM structure determination. Nat. Methods *14*, 290–296.

Raj, V.S., Mou, H., Smits, S.L., Dekkers, D.H., Müller, M.A., Dijkman, R., Muth, D., Demmers, J.A., Zaki, A., Fouchier, R.A., et al. (2013). Dipeptidyl peptidase 4 is a functional receptor for the emerging human coronavirus-EMC. Nature *495*, 251–254.

Ren, W., Qu, X., Li, W., Han, Z., Yu, M., Zhou, P., Zhang, S.Y., Wang, L.F., Deng, H., and Shi, Z. (2008). Difference in receptor usage between severe acute respiratory syndrome (SARS) coronavirus and SARS-like coronavirus of bat origin. J. Virol. *82*, 1899–1907.

Rockx, B., Corti, D., Donaldson, E., Sheahan, T., Stadler, K., Lanzavecchia, A., and Baric, R. (2008). Structural basis for potent cross-neutralizing human monoclonal antibody protection against lethal human and zoonotic severe acute respiratory syndrome coronavirus challenge. J. Virol. *82*, 3220–3235.

Rockx, B., Donaldson, E., Frieman, M., Sheahan, T., Corti, D., Lanzavecchia, A., and Baric, R.S. (2010). Escape from human monoclonal antibody neutralization affects in vitro and in vivo fitness of severe acute respiratory syndrome coronavirus. J. Infect. Dis. *201*, 946–955.

Rossen, J.W., de Beer, R., Godeke, G.J., Raamsman, M.J., Horzinek, M.C., Vennema, H., and Rottier, P.J. (1998). The viral spike protein is not involved in the polarized sorting of coronaviruses in epithelial cells. J. Virol. *72*, 497–503.

Scheres, S.H., and Chen, S. (2012). Prevention of overfitting in cryo-EM structure determination. Nat. Methods *9*, 853–854.

Shulla, A., Heald-Sargent, T., Subramanya, G., Zhao, J., Perlman, S., and Gallagher, T. (2011). A transmembrane serine protease is linked to the severe acute respiratory syndrome coronavirus receptor and activates virus entry. J. Virol. *85*, 873–882.

Song, W., Gui, M., Wang, X., and Xiang, Y. (2018). Cryo-EM structure of the SARS coronavirus spike glycoprotein in complex with its host cell receptor ACE2. PLoS Pathog. *14*, e1007236.

Steinhauer, D.A. (1999). Role of hemagglutinin cleavage for the pathogenicity of influenza virus. Virology *258*, 1–20.

Sui, J., Li, W., Murakami, A., Tamin, A., Matthews, L.J., Wong, S.K., Moore, M.J., Tallarico, A.S., Olurinde, M., Choe, H., et al. (2004). Potent neutralization of severe acute respiratory syndrome (SARS) coronavirus by a human mAb to S1 protein that blocks receptor association. Proc. Natl. Acad. Sci. USA *101*, 2536–2541.

Suloway, C., Pulokas, J., Fellmann, D., Cheng, A., Guerra, F., Quispe, J., Stagg, S., Potter, C.S., and Carragher, B. (2005). Automated molecular microscopy: the new Leginon system. J. Struct. Biol. *151*, 41–60.

Tegunov, D., and Cramer, P. (2019). Real-time cryo-electron microscopy data preprocessing with Warp. Nat. Methods *16*, 1146–1152.

Tian, X., Li, C., Huang, A., Xia, S., Lu, S., Shi, Z., Lu, L., Jiang, S., Yang, Z., Wu, Y., and Ying, T. (2020). Potent binding of 2019 novel coronavirus spike protein by a SARS coronavirus-specific human monoclonal antibody. Emerg. Microbes Infect. *9*, 382–385.

Tortorici, M.A., and Veesler, D. (2019). Structural insights into coronavirus entry. Adv. Virus Res. *105*, 93–116.

Tortorici, M.A., Walls, A.C., Lang, Y., Wang, C., Li, Z., Koerhuis, D., Boons, G.J., Bosch, B.J., Rey, F.A., de Groot, R.J., and Veesler, D. (2019). Structural basis for human coronavirus attachment to sialic acid receptors. Nat. Struct. Mol. Biol. *26*, 481–489.

Traggiai, E., Becker, S., Subbarao, K., Kolesnikova, L., Uematsu, Y., Gismondo, M.R., Murphy, B.R., Rappuoli, R., and Lanzavecchia, A. (2004). An efficient method to make human monoclonal antibodies from memory B cells: potent neutralization of SARS coronavirus. Nat. Med. *10*, 871–875.

Vlasak, R., Luytjes, W., Spaan, W., and Palese, P. (1988). Human and bovine coronaviruses recognize sialic acid-containing receptors similar to those of influenza C viruses. Proc. Natl. Acad. Sci. USA *85*, 4526–4529.

Walls, A.C., Tortorici, M.A., Bosch, B.J., Frenz, B., Rottier, P.J.M., DiMaio, F., Rey, F.A., and Veesler, D. (2016a). Cryo-electron microscopy structure of a coronavirus spike glycoprotein trimer. Nature *531*, 114–117.

Walls, A.C., Tortorici, M.A., Frenz, B., Snijder, J., Li, W., Rey, F.A., DiMaio, F., Bosch, B.J., and Veesler, D. (2016b). Glycan shield and epitope masking of a coronavirus spike protein observed by cryo-electron microscopy. Nat. Struct. Mol. Biol. *23*, 899–905.

Walls, A., Tortorici, M.A., Bosch, B.J., Frenz, B., Rottier, P.J., DiMaio, F., Rey, F.A., and Veesler, D. (2017a). Crucial steps in the structure determination of a coronavirus spike glycoprotein using cryo-electron microscopy. Protein Sci. *26*, 113–121.

Walls, A.C., Tortorici, M.A., Snijder, J., Xiong, X., Bosch, B.-J., Rey, F.A., and Veesler, D. (2017b). Tectonic conformational changes of a coronavirus spike glycoprotein promote membrane fusion. Proc. Natl. Acad. Sci. USA *114*, 11157–11162.

Walls, A.C., Xiong, X., Park, Y.J., Tortorici, M.A., Snijder, J., Quispe, J., Cameroni, E., Gopal, R., Dai, M., Lanzavecchia, A., et al. (2019). Unexpected Receptor Functional Mimicry Elucidates Activation of Coronavirus Fusion. Cell *176*, 1026–1039.

Wan, Y., Shang, J., Graham, R., Baric, R.S., and Li, F. (2020). Receptor recognition by novel coronavirus from Wuhan: An analysis based on decade-long structural studies of SARS. J. Virol. Published online January 29, 2020. https://doi.org/10.1128/JVI.00127-20.

Wang, M., Yan, M., Xu, H., Liang, W., Kan, B., Zheng, B., Chen, H., Zheng, H., Xu, Y., Zhang, E., et al. (2005). SARS-CoV infection in a restaurant from palm civet. Emerg. Infect. Dis. *11*, 1860–1865.

Wang, Q., Qi, J., Yuan, Y., Xuan, Y., Han, P., Wan, Y., Ji, W., Li, Y., Wu, Y., Wang, J., et al. (2014). Bat origins of MERS-CoV supported by bat coronavirus HKU4 usage of human receptor CD26. Cell Host Microbe *16*, 328–337.

Wang, R.Y., Song, Y., Barad, B.A., Cheng, Y., Fraser, J.S., and DiMaio, F. (2016). Automated structure refinement of macromolecular assemblies from cryo-EM maps using Rosetta. eLife *5*, e17219.

Wong, S.K., Li, W., Moore, M.J., Choe, H., and Farzan, M. (2004). A 193-amino acid fragment of the SARS coronavirus S protein efficiently binds angiotensin-converting enzyme 2. J. Biol. Chem. *279*, 3197–3201.

Wong, A.H.M., Tomlinson, A.C.A., Zhou, D., Satkunarajah, M., Chen, K., Sharon, C., Desforges, M., Talbot, P.J., and Rini, J.M. (2017). Receptor-binding loops in alphacoronavirus adaptation and evolution. Nat. Commun. *8*, 1735.

Wrapp, D., Wang, N., Corbett, K.S., Goldsmith, J.A., Hsieh, C.L., Abiona, O., Graham, B.S., and McLellan, J.S. (2020). Cryo-EM structure of the 2019-nCoV spike in the prefusion conformation. Science. Published online February 19, 2020. https://doi.org/10.1126/science.abb2507.

Wu, K., Li, W., Peng, G., and Li, F. (2009). Crystal structure of NL63 respiratory coronavirus receptor-binding domain complexed with its human receptor. Proc. Natl. Acad. Sci. USA *106*, 19970–19974.

Xiong, X., Tortorici, M.A., Snijder, J., Yoshioka, C., Walls, A.C., Li, W., McGuire, A.T., Rey, F.A., Bosch, B.J., and Veesler, D. (2018). Glycan shield and fusion activation of a deltacoronavirus spike glycoprotein fine-tuned for enteric infections. J. Virol. *92*, e01628-17.

Yang, Y., Du, L., Liu, C., Wang, L., Ma, C., Tang, J., Baric, R.S., Jiang, S., and Li, F. (2014). Receptor usage and cell entry of bat coronavirus HKU4 provide insight into bat-to-human transmission of MERS coronavirus. Proc. Natl. Acad. Sci. USA *111*, 12516–12521.

Yang, X.L., Hu, B., Wang, B., Wang, M.N., Zhang, Q., Zhang, W., Wu, L.J., Ge, X.Y., Zhang, Y.Z., Daszak, P., et al. (2015a). Isolation and Characterization of a Novel Bat Coronavirus Closely Related to the Direct Progenitor of Severe Acute Respiratory Syndrome Coronavirus. J. Virol. *90*, 3253–3256.

Yang, Y., Liu, C., Du, L., Jiang, S., Shi, Z., Baric, R.S., and Li, F. (2015b). Two Mutations Were Critical for Bat-to-Human Transmission of Middle East Respiratory Syndrome Coronavirus. J. Virol. *89*, 9119–9123.

Yuan, Y., Cao, D., Zhang, Y., Ma, J., Qi, J., Wang, Q., Lu, G., Wu, Y., Yan, J., Shi, Y., et al. (2017). Cryo-EM structures of MERS-CoV and SARS-CoV spike glycoproteins reveal the dynamic receptor binding domains. Nat. Commun. *8*, 15092.

Zaki, A.M., van Boheemen, S., Bestebroer, T.M., Osterhaus, A.D., and Fouchier, R.A. (2012). Isolation of a novel coronavirus from a man with pneumonia in Saudi Arabia. N. Engl. J. Med. *367*, 1814–1820.

Zhang, H., Wang, G., Li, J., Nie, Y., Shi, X., Lian, G., Wang, W., Yin, X., Zhao, Y., Qu, X., et al. (2004). Identification of an antigenic determinant on the S2 domain of the severe acute respiratory syndrome coronavirus spike glycoprotein capable of inducing neutralizing antibodies. J. Virol. *78*, 6938–6945.

Zhou, P., Yang, X.L., Wang, X.G., Hu, B., Zhang, L., Zhang, W., Si, H.R., Zhu, Y., Li, B., Huang, C.L., et al. (2020). A pneumonia outbreak associated with a new coronavirus of probable bat origin. Nature. Published online February 3, 2020. https://doi.org/10.1038/s41586-020-2012-7.

Zhu, N., Zhang, D., Wang, W., Li, X., Yang, B., Song, J., Zhao, X., Huang, B., Shi, W., Lu, R., et al. (2020). A Novel Coronavirus from Patients with Pneumonia in China, 2019. N Engl J Med. *382*, 727–733.

Zivanov, J., Nakane, T., Forsberg, B.O., Kimanius, D., Hagen, W.J., Lindahl, E., and Scheres, S.H. (2018). New tools for automated high-resolution cryo-EM structure determination in RELION-3. eLife *7*, e42166.

Zivanov, J., Nakane, T., and Scheres, S.H.W. (2019). A Bayesian approach to beam-induced motion correction in cryo-EM single-particle analysis. IUCrJ *6*, 5–17.

STAR★METHODS

KEY RESOURCES TABLE

REAGENT or RESOURCE	SOURCE	IDENTIFIER
Antibodies		
AlexaFluor680-conjugated AffiniPure Goat Anti Human IgG	JacksonImmuno	Cat# 109-625-098 Lot# 139337
Biological Samples		
57BL/6J Mice	Jackson Laboratory	Cat# 000664
Chemicals, Peptides, and Recombinant Proteins		
Thrombin	EMD Millipore	Ref# 605195 Lot# 2946006
One-GloEX	Promega	Cat# E8110
293-Free Transfection Reagent	Millipore Sigma	Cat# 72181
Lipofectamine-2000 Transfection Reagent	ThermoFisher	Cat# 11668500
Adjuvant	Sigma-Aldrich	Cat# S6322
Deposited Data		
SARS-CoV-2 S CryoEM maps	This Paper	EMD: 21452, EMD: 21457
SARS-CoV-2 S atomic models	This Paper	PDB: 6VXX, PDB: 6VYB
Experimental Models: Cell Lines		
Freestyle HEK293	ThermoFisher	Cat# R79007
HEK293T/17 adherent	Millet and Whittaker, 2016	ATCC CRL-11268
Vero(C1008)E6 adherent	ECACC General Collection	Cat# 85020206
Baby Hamster Kidney (BHK)	ATCC	Cat# CCL-10 Lot# 70009857
Recombinant DNA		
pCMV-SARS-CoV-2 S 2P furin cleavage mutation	Genscript	N/A
pcD5 - ACE2	Raj et al., 2013	N/A
pcDNA3.1- SARS-CoV-2 S^B	Genscript	N/A
pcDNA3.1- SARS-CoV S^B	This paper	N/A
pcDNA3.1(-) –Full-length wild-type SARS-CoV-2 S	Genscript	N/A
pcDNA3.1(-) –Full-length wild-type SARS-CoV S	Millet and Whittaker, 2016	N/A
pCMV-murine leukemia virus gag-pol	Millet and Whittaker, 2016	N/A
pTG-Luciferase	Millet and Whittaker, 2016	N/A
Software and Algorithms		
UCSF Chimera	Goddard et al., 2007	https://www.rbvi.ucsf.edu/chimera/
UCSF ChimeraX	Goddard et al., 2018	https://www.rbvi.ucsf.edu/chimerax/
Coot	Emsley et al., 2010	https://www2.mrc-lmb.cam.ac.uk/personal/pemsley/coot/
Relion	Scheres and Chen, 2012; Zivanov et al., 2019	https://www2.mrc-lmb.cam.ac.uk/relion/index.php?title=Main_Page
Rosetta	Frenz et al., 2019; Wang et al., 2016	https://www.rosettacommons.org/software
Leginon	Suloway et al., 2005	http://emg.nysbc.org/redmine/projects/leginon/wiki/Leginon_Homepage
WARP	Tegunov and Cramer, 2019	https://github.com/cramerlab/warp
CryoSPARC	Punjani et al., 2017	https://cryosparc.com
MolProbity	Chen et al., 2010	http://molprobity.biochem.duke.edu/

(*Continued on next page*)

Continued

REAGENT or RESOURCE	SOURCE	IDENTIFIER
Other		
Octet Red	ForteBio, Pall LLC	https://www.fortebio.com/products/label-free-bli-detection/8-channel-octet-systems
Anti-Penta-HIS (HIS1K)	ForteBio, Pall LLC	Part# 18-5120 Lot# 1910224A
HisTALON Superflow cartridge	Takara	Cat# 635683 Lot# 1509573A
HiTrap Protein A HP	GE Life Sciences	Cat# 29-0485-76
Superose 6 Increase 10/300	GE Life Sciences	Cat# 29-0915-96 Lot# 10226998
Lacey Formvar/Carbon 400 mesh, Cu Grids	Ted Pella	Prod# 01885-F Lot# 020218

LEAD CONTACT AND MATERIALS AVAILABILITY

Further information and requests for resources and reagents should be directed to and will be fulfilled by the Lead Contact David Veesler (dveesler@uw.edu).

The unique/stable reagents generated in this study are available from the Lead Contact with a completed Materials Transfer Agreement.

The number of replicates carried out for each experiment is described in the figure/table legends.

EXPERIMENTAL MODEL AND SUBJECT DETAILS

Cell lines

HEK293F is a female human embryonic kidney cell line transformed and adapted to grow in suspension (Life Technologies). HEK293F cells were grown in 293FreeStyle expression medium (Life Technologies), cultured at 37°C with 8% CO_2 and 130 rpm. HEK293T/17 is a female human embryonic kidney cell line (ATCC). VeroE6 is a female kidney epithelial cell from African green monkey. BHK is a kidney cell line from baby hamsters. All adherent cells were cultured at 37°C with 8% CO2 in flasks with DMEM + 10% FBS + 1% penicillin-streptomycin. Cells lines were not tested for mycoplasma contamination nor authenticated.

METHOD DETAILS

Transient expression of SARS-CoV-2 and SARS-CoV S^B

The SARS-CoV S^B construct was cloned from a SARS-CoV S ectodomain (Walls et al., 2019) synthesized by GeneArt (ThermoFisher Scientific) into a modified pOPING vector with an N-terminal mu-phosphatase signal peptide and a C-terminal hexa-histidine tag (G-HHHHHH). The boundaries of the construct are N-terminal $_{306}$RVVPSG$_{311}$ and C-terminal $_{571}$LDISP$_{5975}$. The SARS-CoV-2 S^B construct was synthesized by GenScript into pcDNA3.1- with an N-terminal mu-phosphatase signal peptide and a C-terminal hexa-histidine tag (G-HHHHHH). The boundaries of the construct are N-terminal $_{328}$RFPN$_{331}$ and C-terminal $_{530}$STNL$_{533}$. Both constructs were produced in 500mL HEK293F cells grown in suspension using FreeStyle 293 expression medium (Life technologies) at 37°C in a humidified 8% CO_2 incubator rotating at 130 rpm. The cultures were transfected using 293-Free transfection reagent (Millipore) with cells grown to a density of 1 million cells per mL and cultivated for 3–4 days. The supernatants were harvested and cells resuspended for another 3–4 days, yielding two harvests. Proteins were purified from clarified supernatants using a 5mL Cobalt affinity column (Takara), concentrated and flash frozen in a buffer containing 20 mM Tris pH 8.0 and 300 mM NaCl prior to analysis. SDS-PAGE was run to check purity.

Transient expression of hACE2

Expression and purification of human angiotensin-converting enzyme ectodomain (ACE2, residues 1–614) fused to the Fc region of human IgG (hFc) was performed as previously described (Walls et al., 2019) and cleavage of the Fc fragment was carried out with thrombin. Briefly, hACE2 was produced in 500mL HEK293F cells grown in suspension using FreeStyle 293 expression medium (Life technologies) at 37°C in a humidified 8% CO_2 incubator rotating at 130 rpm. The cultures were transfected using 293-Free transfection reagent (Millipore) with cells grown to a density of 1 million cells per mL and cultivated for 4 days. The supernatants were harvested and cells resuspended for another four days, yielding two harvests. Clarified supernatants were concentrated using Vivaflow tangential filtration cassettes (Sartorius, 10-kDa cut-off) before affinity purification using a Protein A column (GE

LifeSciences) followed by gel filtration chromatography using a Superdex 200 10/300 GL column (GE Life Sciences) equilibrated in 20 mM Tris-HCl, pH 8.0, 100 mM NaCl. The Fc tag was removed by thrombin cleavage in a reaction mixture containing 3 mg of recombinant ACE2-FC ectodomain and 10 μg of thrombin in 20 mMTris-HCl pH8.0, 150 mM NaCl and 2.5 mM $CaCl_2$.The reaction mixture was incubated at 25°C overnight and re-loaded in a Protein A column to remove uncleaved protein and the Fc tag. The cleaved protein was further purified by gel filtration using a Superdex 200 column 10/300 GL (GE Life Sciences) equilibrated in a buffer containing 20 mM Tris pH 8.0 and 100 mM NaCl. The purified protein was quantified using absorption at 280 nm and concentrated to approximately 1 mg/mL·

Pseudovirus production

MLV-based SARS-CoV S, SARS-CoV-2 S, and SARS-CoV-2 $S_{fur/mut}$ pseudotypes were prepared as previously described (Millet and Whittaker, 2016). HEK293T cells were co-transfected using Lipofectamine 2000 (Life Technologies) with an S encoding-plasmid, an MLV Gag-Pol packaging construct and the MLV transfer vector encoding a luciferase reporter, according to the manufacturer's instructions. Cells were incubated for 5 h at 37°C with transfection medium. Cells were then washed with DMEM two times and then DMEM containing 10% FBS was added for 60 h. The supernatants were then harvested and filtered through 0.45-mm membranes, concentrated with a 30kDa membrane for 10 min at 3,000 rpm and then frozen at −80°C.

Western Blotting

SARS-CoV S, SARS-CoV-2 S, and SARS-CoV-2 $S_{fur/mut}$ pseudovirions were thawed and 4X SDS loading buffer was added prior to boiling for 10 min at 95°C. Samples were run on a 4%–20% gradient Tris-Glycine Gel (BioRad) and transferred to a PVDF membrane. An anti-S_2 SARS-CoV S monoclonal primary antibody (1:150 dilution) and an Alexa Fluor 680-conjugated goat anti-human or mouse secondary antibody (1:30,000 and 1:15,000 dilution respectively, Jackson Laboratory) were used for Western-blotting. A LI-COR processor was used to develop images.

Pseudovirus entry assays

VeroE6 and BHK cells were cultured in 10% FBS, 1% PenStrep DMEM. BHK or VeroE6 cells were plated into 12 well plates at a density of 0.3×10^6 for 16 h. BHK cells were either not transfected or transfected with 0.8 μg ACE2 per well using standard lipofectamine2000 (Life Technologies) protocols and incubated for another 16 h. 20uL of concentrated pseudovirus was added to the wells after washing three times with DMEM. After 2-3 h, 20% FBS and 2% PenStrep containing DMEM was added to the cells for 48 h. Following the 48-h infection, One-Glo-EX (Promega) was added to the cells in equivalent culturing volume and incubated in the dark for 10 min prior to reading on a Varioskan LUX plate reader (ThermoFisher). For entry inhibition assays, 1:100 diluted plasma was incubated with an equal amount of pseudovirus for 30 min at room temperature prior to infection with normalized amounts of pseudovirus added to the cells. Measurements were done in triplicate and relative luciferase units (RLU) were plotted.

Biolayer interferometry

Assays were performed on an Octet Red (ForteBio) instrument at 30°C with shaking at 1,000 RPM. Anti-penta His biosensors were hydrated in water for 30 min prior to a 1 min incubation in 10X kinetics buffer (undiluted). Either SARS-CoV-2 S^B or SARS-CoV S^B were loaded at 10-20 μg/mL in 10X Kinetics Buffer for 200-900 s prior to baseline equilibration for 180 s in 10X kinetics buffer. Association of ACE2 in 10X kinetics buffer at various concentrations in a two-fold dilution series from 20nM to 2.5nM was carried out for 1,000 s prior to dissociation for 1,000 s. The data were baseline subtracted prior to fitting performed using a 1:1 binding model and the ForteBio data analysis software. Mean k_{on}, k_{off} values were determined with a global fit applied to all data. The experiments were done with two separate purification batches of SARS-CoV S^B, SARS-CoV-2-S^B, and ACE2 each in duplicate and the average is reported.

Protein expression and purification

The SARS-CoV-2 2P S (GenBank: YP_009724390.1) ectodomain was produced in 500mL HEK293F cells grown in suspension using FreeStyle 293 expression medium (Life technologies) at 37°C in a humidified 8% CO2 incubator rotating at 130 rpm The culture was transfected using 293fectin (ThermoFisher Scientific) with cells grown to a density of 1 million cells per mL and cultivated for three days. The supernatant was harvested and cells resuspended for another three days, yielding two harvests. Clarified supernatants were purified using a 5mL Cobalt affinity column (Takara). Purified protein was filtered or concentrated and flash frozen in a buffer containing 20 mM Tris pH 8.0 and 150 mM NaCl prior to cryoEM analysis.

CryoEM sample preparation and data collection

3 μL of 0.16 mg/mL SARS-CoV-2 S was loaded onto a freshly glow discharged (30 s at 20 mA) lacey carbon grid with a thin layer of evaporated continuous carbon prior to plunge freezing using a vitrobot MarkIV (ThermoFisher Scientific) using a blot force of −1 and 2.5 s blot time at 100% humidity and 25°C. Data were acquired using the Leginon software (Suloway et al., 2005) to control an FEI Titan Krios transmission electron microscope operated at 300 kV and equipped with a Gatan K2 Summit direct detector and Gatan Quantum GIF energy filter, operated in zero-loss mode with a slit width of 20 eV. Automated data collection was carried out using Leginon at a nominal magnification of 130,000x with a pixel size of 0.525 Å. The dose rate was adjusted to 8

counts/pixel/s, and each movie was acquired in super-resolution mode fractionated in 50 frames of 200 ms. 4,500 micrographs were collected in a single session with a defocus range comprised between 1.0 and 2.5 μm.

Cryo-EM data processing

Movie frame alignment, estimation of the microscope contrast-transfer function parameters, particle picking and extraction were carried out using Warp (Tegunov and Cramer, 2019). Particle images were extracted with a box size of 800 binned to 400 yielding a pixel size of 1.05 Å. For each dataset two rounds of reference-free 2D classification were performed using cryoSPARC (Punjani et al., 2017) to select well-defined particle images. Subsequently, two rounds of 3D classification with 50 iterations each (angular sampling 7.5° for 25 iterations and 1.8° with local search for 25 iterations) were carried out using Relion (Zivanov et al., 2018) without imposing symmetry to separate distinct SARS-CoV-2 S conformations. 3D refinements were carried out using non-uniform refinement along with per-particle defocus refinement in cryoSPARC (Punjani et al., 2017) using an *ab initio* model generated using cryoSPARC. Particle images were subjected to Bayesian polishing (Zivanov et al., 2019) before performing another round of non-uniform refinement in cryoSPARC (Punjani et al., 2017) followed by per-particle defocus refinement and again non-uniform refinement. Local resolution estimation, filtering and sharpening was carried out using CryoSPARC. Reported resolutions are based on the gold-standard Fourier shell correlation (FSC) of 0.143 criterion and Fourier shell correlation curves were corrected for the effects of soft masking by high-resolution noise substitution (Scheres and Chen, 2012).

CryoEM model building and analysis

UCSF Chimera (Goddard et al., 2007) and Coot were used to fit atomic models (PDB 6NB6) into the cryoEM map. The model was subsequently manually rebuilt using Coot and the C3-symmetrized map (Brown et al., 2015; Emsley et al., 2010). This model was then used to build features specific of the C1-map. N-linked glycans were hand-built into the density where visible and the models were refined and relaxed using Rosetta (Wang et al., 2016). Glycan refinement relied on a dedicated Rosetta protocol, which uses physically realistic geometries based on prior knowledge of saccharide chemical properties (Frenz et al., 2019), and was aided by using both sharpened and unsharpened maps. Models were analyzed using MolProbity (Chen et al., 2010), EMringer (Barad et al., 2015), Phenix (Liebschner et al., 2019) and privateer (Agirre et al., 2015) to validate the stereochemistry of both the protein and glycan components (Table S1). Figures were generated using UCSF ChimeraX (Goddard et al., 2018) and consurf (Ashkenazy et al., 2016).

Immunizations with SARS-CoV S

57BL/6J mice were obtained from the Jackson Laboratory and maintained at the Comparative Medicine Facility at the Fred Hutchinson Cancer Research Center. After collecting a pre-bleed, mice were immunized with 5μg of SARS-CoV 2P S ectodomain trimer (this construct was previously described (Walls et al., 2019)) formulated in 50μl of PBS and 50μl of Sigma Adjuvant System subcutaneously in the base of the tail at weeks 0, 4, and 12 and bleeds were collected 2 weeks after each immunization. Plasma from immunized animals was heat inactivated at 56°C for 1 h and then stored at 4°C until use. All experiments were conducted at the Fred Hutchinson Cancer Research Center according to approved Institutional Animal Care and Use Committee protocols.

QUANTIFICATION AND STATISTICAL ANALYSIS

Western-blots and biolayer interferometry assays were performed multiple times with at least two independent preparations of each sample.

No methods were used to determine whether the data met assumptions of the statistical approach.

DATA AND CODE AVAILABILITY

The cryoEM maps and atomic models have been deposited at the Electron Microscopy Data Bank and the Protein Data Bank with accession codes EMD: 21452 and PDB: 6VXX (closed SARS-CoV-2 S), as well as EMD: 21457 and PDB: 6VYB (SARS-CoV-2 S with one S^B open). A list of software used in this study can be found in the Key Resources Table.

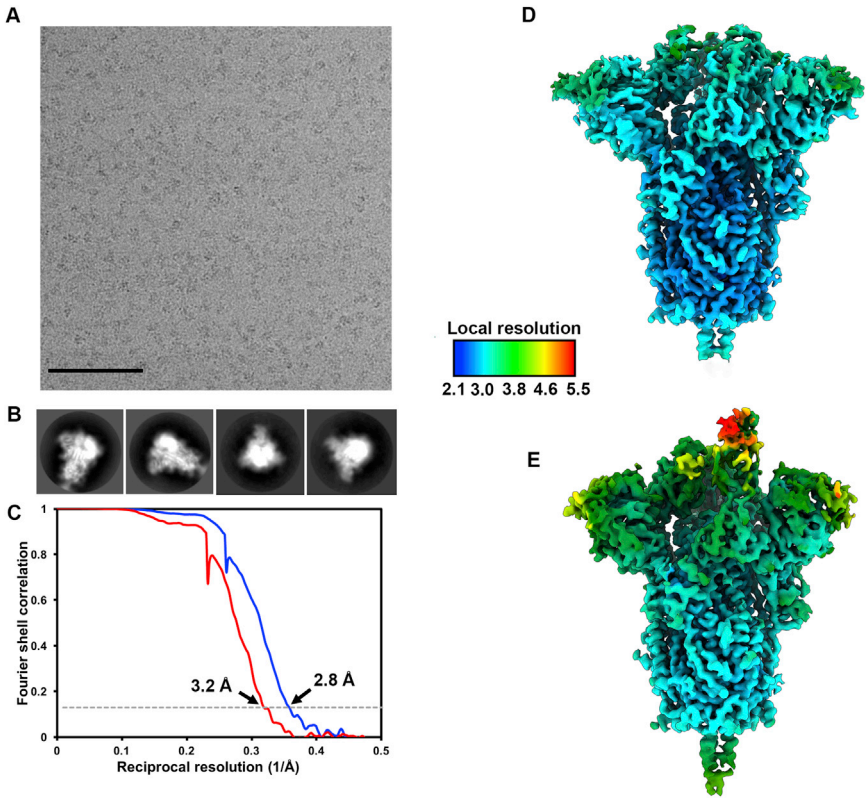

Figure S1. Cryo-EM Data Processing and Validation, Related to Figures 3, 4, and 5

A-B. Representative electron micrograph (A) and class averages (B) of SARS-CoV-2 S embedded in vitreous ice. Scale bar: 100nm. C. Gold-standard Fourier shell correlation curves for the closed (blue) and partially open trimers (red). The 0.143 cutoff is indicated by horizontal dashed lines. D-E. Local resolution map calculated using cryoSPARC for the closed (D) and partially open (E) reconstructions.

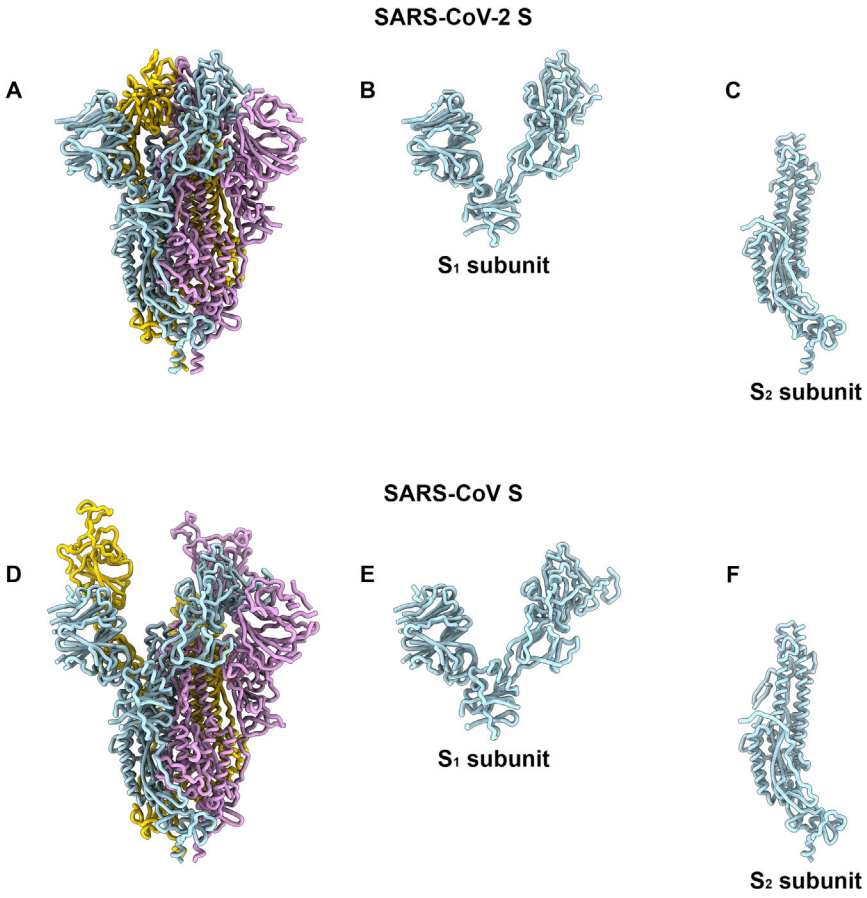

Figure S2. Comparison of the SARS-CoV-2 and SARS-CoV S Structures, Related to Figures 3, 4, and 5

Ribbon diagrams of the SARS-CoV-2 S (A) and SARS-CoV S (PDB 6NB6, D) ectodomain cryoEM structures. The SARS-CoV-2 (B) and SARS-CoV (E) S_1 subunits. The SARS-CoV-2 (C) and SARS-CoV (F) S_2 subunits.